Journal of Hydrology 475 (2012) 204–228

Contents lists available at SciVerse ScienceDirect

Journal of Hydrology

journal homepage: www.elsevier.com/locate/jhydrol

# Using discrete wavelet transforms to analyze trends in streamflow and precipitation in Quebec and Ontario (1954–2008)

D. Nalley, J. Adamowski, B. Khalil *

*Department of Bioresource Engineering, Faculty of Agriculture and Environmental Sciences, McGill University, Macdonald Stewart Building, 21111 Lakeshore Road, Ste-Anne-de-Bellevue, Quebec, Canada H9X 3V9*

ARTICLE INFO

*Article history:*
Received 15 May 2012
Received in revised form 9 September 2012
Accepted 25 September 2012
Available online 4 October 2012
This manuscript was handled by Andras Bardossy, Editor-in-Chief, with the assistance of Efrat Morin, Associate Editor

*Keywords:*
Trend detection
Streamflow
Precipitation
Discrete wavelet transform
Mann–Kendall trend test

SUMMARY

This paper aims to detect trends in mean flow and total precipitation data over southern parts of Quebec and Ontario, Canada. The main purpose of the trend assessment is to find out what time scales are affecting the trends observed in the datasets used. In this study, a new trend detection method for hydrological studies is explored, which involves the use of wavelet transforms (WTs) in order to separate the rapidly and slowly changing events contained in a time series. More specifically, this study co-utilizes the Discrete Wavelet Transform (DWT) technique and the Mann–Kendall (MK) trend tests to analyze and detect trends in monthly, seasonally-based, and annual data from eight flow stations and seven meteorological stations in southern Ontario and Quebec during 1954–2008. The combination of the DWT and MK test in analyzing trends has not been extensively explored to date, especially in detecting trends in Canadian flow and precipitation time series. The mother wavelet type and the extension border used in the wavelet transform, as well as the number of decomposition levels, were determined based on two criteria. The first criterion is the mean relative error of the wavelet approximation series and the original time series. In addition, a new criterion is proposed and explored in this study, which is based on the relative error of the MK *Z*-values of the approximation component and the original time series. Sequential Mann–Kendall analysis on the different wavelet detail components (with their approximation component added) that result from the time series decomposition was also used and found to be helpful because it depicts how harmonious each of the detail components (plus approximation) is with respect to the original data. This study found that most of the trends are positive and started during the mid-1960s to early 1970s. The results from the wavelet analysis and Mann–Kendall tests on the different data types (using the 5% significance level) reveal that in general, intra- and inter-annual events (up to 4 years) are more influential in affecting the observed trends.

© 2012 Elsevier B.V. All rights reserved.

## 1. Introduction

The intensification of the hydrologic cycle is one of the most evident effects caused by climate warming (Ampitiyawatta and Guo, 2009; Zhang et al., 2009; Durdu, 2010). Changes in hydrological processes may in turn affect the overall availability and quality of water resources, and alter the spatiotemporal characteristics of hydrologic occurrences, such as the timing of flow events, and the frequency and severity of floods and droughts (Mishra and Singh, 2010; Burn et al., 2010). High-latitude areas have been projected to experience more severe impacts associated with climate change (Zhang et al., 2001). Labat et al. (2004) who studied the global and continental runoff associated with temperature increases found that North America is very vulnerable to recent climate change. One of the most significant consequences of temperature increases and changes in precipitation patterns is the dramatic modification of the hydrologic regimes of northern rivers (Boyer et al., 2010).

The impacts of changing climate in Canada vary from one area to another and have been studied by numerous authors, both at the national and regional scale. Studies on trends of various hydro-climatic indices reveal a variety of results; both positive and negative trends were found across different parts of Canada. According to Ehsanzadeh et al. (2011), who analyzed Canadian low flows, there is a positive trend in winter low flows (including in eastern Canada), but the trends are negative in western Canada. Summer low flows are found to exhibit positive trends in central Canada, but the trends are negative in regions such as eastern Ontario and Quebec (Ehsanzadeh et al., 2011). Similarly, Adamowski and Bocci (2001) found that there is a significant positive trend in the yearly low flow in western Quebec and southern Ontario;

* Corresponding author. Tel.: +1 514 398 7614; fax: +1 514 398 8387.
*E-mail addresses:* deasy.nalley@mail.mcgill.ca (D. Nalley), jan.adamowski@mcgill.ca (J. Adamowski), bahaa.khalil@mail.mcgill.ca, bahaa_khalil@rocketmail.com (B. Khalil).

0022-1694/$ - see front matter © 2012 Elsevier B.V. All rights reserved.
http://dx.doi.org/10.1016/j.jhydrol.2012.09.049

however, the opposite was observed for central and eastern Canada for the same variable. The latest assessment by the Intergovernmental Panel on Climate Change (IPCC) also stated that annual precipitation has increased over much of North America, especially in northern Canada, but has decreased in the Canadian Prairies (IPCC, 2007). Recent changes in annual total precipitations in Canada were between −10% and +35% (Zhang et al., 2001).

One of the predicted effects of climate change in Quebec is the increase in the intensity and frequency of heavy floods, resulting from heavy precipitation (Assani et al., 2010). McBean and Motiee (2006) also found that there are significant upward trends at the 5%-level in flow and precipitation for the Great Lakes watershed over the period of 1930–1990. These findings are relatively consistent with the predictions of the General Circulation Models (GCMs) for the year 2050 (McBean and Motiee, 2006). The results of the Canadian General Circulation Model (CGCMI) and a coupled hydrologic–hydraulic model used by Roy et al. (2001) predicted that the magnitude of heavy precipitation occurrences will increase significantly in Quebec; and Burn and Hag Elnur (2002) observed that annual maximum flows were increasing in southern Quebec (the Great Lakes and St. Lawrence areas). Zhang et al. (2000) found that the annual precipitation has gone up by between 5% and 35% in southern Canada for the period of 1900–1998. Using a hydrological model on different future climatic scenarios (based on greenhouse gas emission scenarios), Boyer et al. (2010) also projected that in the next 100 years there will be changes in river discharges for both the north and south shores of the St. Lawrence River.

It is not surprising that many of the arguments made concerning both climate variability and climatic change are directly related to the detection of trends (or lack thereof) in hydro-climatic parameters such as temperature, precipitation, and streamflow (Birsan et al., 2005). Changes in the patterns and other characteristics of precipitation caused by the daily, seasonal, yearly, and decadal variations should be monitored because they have important ramifications (Ampitiyawatta and Guo, 2009). It is therefore essential to investigate trends associated with hydrological events in order to better assess the potential future impacts of climatic change on water resources (e.g. at the regional level). Hydrologic variables are also regarded as useful indicators of how the climate has changed and varied over time (Burn and Hag Elnur, 2002). It has been suggested that public policies tailored to consider the effects of regional climate change could be modified to cater for a specific ecozone. This would take into account knowledge of local climatic and hydrological trends, rather than general patterns of global climate change (Clark et al., 2000).

One way to accomplish trend assessments is through time-series analysis. Using observational data instead of the output of a model minimizes the uncertainties associated with the modelling process such as assumption concept simplifications (Svensson et al., 2005). Studies have applied several methods to detect and quantify trends in precipitation and streamflow data. Some of the more common methods found in the recent literature involve the use of the bootstrap methods (Adamowski and Bougadis, 2003; Cunderlik and Burn, 2004; Abdul Aziz and Burn, 2006; Burn et al., 2010); regression models (Svensson et al., 2005; Shao et al., 2010; Timofeev and Sterin, 2010); and non-parametric statistical tests (Birsan et al., 2005; Zhang et al., 2009, 2010; Durdu, 2010; Liu et al., 2010). The Mann–Kendall (MK) trend test (Mann, 1945; Kendall, 1975) is probably the most widely used non-parametric test in detecting monotonic trends (Yue and Pilon, 2004; Hamed, 2008). The most attractive features of this test are that it is powerful even for skewed distributions (Önöz and Bayazit, 2003), simple to compute, and resilient to non-stationary data and missing values (Partal and Küçük, 2006; Adamowski et al., 2009). A noticeable weakness of the MK test is that it does not account for serial correlation, which is very often found in precipitation and streamflow data (Hamed and Rao, 1998; Partal and Küçük, 2006). McBean and Motiee (2006) also specified that the MK test may not necessarily detect non-linear trends. As a result, the MK test is often used in conjunction with other methods or models for trend-related studies in hydrology.

More recently, the wavelet transform – a relatively recent development in signal processing – has also emerged as a tool used in trend analysis (Wang et al., 2011). Wavelet transform has a major advantage over classical signal analysis techniques such as the Fourier Transform, which only uses a single-window analysis, resulting in time-averaged results that lose their temporal information (Torrence and Compo, 1998; Drago and Boxall, 2002). The main issue with the fixed window size used in the Windowed Fourier Transform is that it loses the time localization at high frequencies when the window is sliding along the time series because there are too many oscillations captured within the window. It also loses the frequency localization at low frequencies because there is only a few low-frequency oscillations included in the window (Santos et al., 2001). The wavelet transform can handle these issues by decomposing a one-dimensional signal into two-dimensional time–frequency domains at the same time (Adamowski et al., 2009). Unlike sine waves, which are the main functions used in Fourier analysis, wavelets are usually irregular and asymmetric in shape. This property makes a wavelet ideal for analyzing signals that contain sharp changes and discontinuities – a localized signal analysis (Quiroz et al., 2011). Wavelet transforms use different window sizes, which are able to compress and stretch wavelets in different scales or widths; these are then used to decompose a time series (Santos et al., 2001). Narrow windows are used to track the high-frequency components or rapidly-changing events of the analyzed signals (which are represented by the lower detail levels), whereas wider window sizes are used to track the signals' low-frequency components including trends (which are represented by the higher detail levels and the approximation component) (Santos et al., 2001; Cannas et al., 2006). Additionally, wavelet analysis is able to show many properties of a time series or data that may not be revealed by other signal analysis techniques, such as trends, discontinuities, change points, and self-similarity. In summary, the wavelet transform is capable of analyzing a wider range of signals more accurately when compared to the Fourier analysis (Nolin and Hall-McKim, 2006; Goodwin, 2008). The results of wavelet analysis can be used to determine the main components or modes in the time series that may contribute to producing trends (Kim, 2004). These results can then be used to examine the temporal patterns of both a signal's frequency and time domains (Labat, 2005; Wang et al., 2011).

Several different studies conducted to analyze trends in streamflow and precipitation in different climate settings have employed the use of wavelet-based methods. Zume and Tarhule (2006) used the continuous wavelet transform and the MK test to analyze the variability of precipitation and streamflow in northwestern Oklahoma for a period of over 100 years. They found that both annual precipitation and streamflow experience inter-annual to decadal variability. Xu et al. (2009) studied the impact of climate change in the Tarim River basin in China for the period of 1959–2006, by approximating non-linear trends in annual temperature, precipitation, and relative humidity time series using a wavelet-based decomposition and reconstruction technique. They found that all variables showed non-linear trends and/or fluctuating patterns, especially at the 4-and 8-year scales. Partal (2010) analyzed streamflow datasets from four stations with different climatic conditions in Turkey, three from the Sakarya basin and one from the Seyhan basin. The study found different scales were responsible for the different trends in different climatic areas. In the Sakarya basin, the real trends were associated with the 16-year periodic component, whereas in the Seyhan basin, the trends were associated with the 4-year and 8-year modes.

The main purpose of this study is to combine the use of the Discrete Wavelet Transform (DWT) technique and the Mann–Kendall trend tests in order to investigate trends in streamflow and precipitation datasets in Ontario and Quebec by analyzing their monthly, seasonally-based, and annual time series. The analysis of monthly to yearly data should allow this study to investigate the rapidly and slowly changing events in the datasets used. The trend analysis is done by examining the behavior and fluctuation of high-frequency and low-frequency components of the available time series, and whether they are contributing to the possible existence of trends in these series. This is important because although research on trend assessment of flow and precipitation has been conducted in different parts of Canada, they have rarely focused on the details of the time-scale fluctuations or cycles that affect the trends in flow and precipitation in Ontario and Quebec. There could be longer cycles than daily or seasonal fluctuations that exist to affect the trends in these variables, which will be explored in this present study. Using the DWT technique in conjunction with the MK test has not been extensively explored to date, in analyzing streamflow and/or precipitation data (especially in Canadian studies). Additionally, a new criterion of using the relative error of the trend values between the original data and the approximation component of the DWT is proposed and successfully applied in this study. The usefulness of this new criterion for the DWT procedure is discussed in detail in Section 4.3.

In this study, the possible existence of significant autocorrelations and seasonality patterns in the data sets used is first checked. Following this, each time series is decomposed via the DWT approach into its appropriate number of decomposition levels (the explanation on how to determine the appropriate number of decomposition levels is provided in Section 4.3). Finally, depending on the characteristics of the analyzed time series (e.g. the presence or absence of significant autocorrelations or seasonality cycles), the most suitable MK test is applied to the original data and the series resulting from the DWT decomposition. Although this type of detailed information is very important to be explored and included in the methodology, it is often overlooked or missing in most published trend detection/estimation studies.

Water resource planners and managers can use the results obtained from this study to address issues in water resources that are associated with climate variability, by creating appropriate policies and strategies. Some potential applications include the implementation of useful adaptation and mitigation strategies as a response to climate change; the optimization of various hydrologic structural designs such as dams and reservoirs; and improvements in stormwater planning (Coats, 2010) and flood protection projects. In addition, in order to improve the forecasting precision of water resources for current and future management, an accurate understanding of the temporal variations of hydrologic variables is vital (Nolin and Hall-McKim, 2006). The authors of this paper believe that the findings from this study can serve as a baseline reference for future research and watershed planning/management, and will advance the understanding of precipitation and streamflow dynamics in Canada and at the smaller, watershed-scale in Quebec and Ontario.

## 2. Theoretical background

### 2.1. Wavelet Transforms (WTs)

A WT is used to mathematically decompose a signal into multiple lower resolution levels by controlling the scaling and shifting factors of a single wavelet – the mother wavelet $\Psi$. This is accomplished by using a high-pass filter and a low-pass filter. A wavelet function is a function having a wave shape and limited but flexible length with a mean value that is equal to zero, and is localized in both time and frequency domains. The term wavelet function generally refers to either orthogonal or non-orthogonal wavelets (Torrence and Compo, 1998).

One of the main reasons to utilize wavelet-based methods in hydrological studies is due to its robust property – it does not involve any possibly incorrect assumptions of distribution and parametric testing protocols (Kisi and Cimen, 2011). The WT also filters out the high-frequency components of a signal (de Artigas et al., 2006). Wavelet transforms involve shifting forward the wavelet in a number of steps along an entire time series, and generating a wavelet coefficient at each step. This measures the level of correlation of the wavelet to the signal in each section. The variation in the coefficients indicates the shifting of similarity of the wavelet with the original signal in time and frequency. This process is then repeated for each scaled version of the wavelet, in order to produce sets of wavelet coefficients at the different scales. The lower scales represent the compressed version of the mother wavelet, and correspond to the rapidly changing features or high-frequency components of the signal. The higher scales are the stretched version of a wavelet, and their wavelet coefficients are identified as slowly changing or low-frequency components of the signal. Therefore, wavelet transforms analyze trends in time series by separating its short, medium, and long-period components (Drago and Boxall, 2002).

WT can be performed using two approaches: Continuous Wavelet Transform (CWT) and Discrete Wavelet Transform (DWT). CWT operates on smooth continuous functions and can detect and decompose signals on all scales. Examples of mother wavelets used in CWT are the Morlet and Paul wavelets, among others. DWT may use mother functions such as the Mallat or à trous algorithms, which operate on scales that have discrete numbers. The scales and locations used in DWT are normally based on a dyadic arrangement (i.e. integer powers of two) (Chou, 2007). DWT is especially useful for time series containing sharp jumps or shifts (Partal and Küçük, 2006). One requirement of DWT is that the mother wavelet has to have an orthogonal basis, while a non-orthogonal wavelet can be used with either DWT or CWT.

#### 2.1.1. Continuous Wavelet Transform (CWT)

For a time series, $x_t$, that has a continuous scale but a discrete recording sequence and $t = 0,\ldots,t-1$, then the wavelet function ($\Psi$), which depends on a time variable ($\eta$), is generally defined as (Partal and Küçük, 2006):

$$\Psi(\eta) = \Psi(s,\gamma) = \frac{1}{\sqrt{s}}\Psi\left(\frac{t-\gamma}{s}\right) \tag{1}$$

where $t$ represents time; variable $\gamma$ is the translation factor (time shift) of the wavelet over the time series; and variable $s$ ranging from 0 to $+\infty$ denotes the wavelet scale (scale factor). When $\gamma = 0$ and $s = 1$, $\Psi(t)$ represents the mother wavelet – all wavelets following this computation are the rescaled (translated and dilated) versions of the mother wavelet. In order to be acceptable as a wavelet, the function $\Psi(\eta)$ has to satisfy the condition of having zero mean (implying the existence of oscillations) and be localized in time–frequency space (Torrence and Compo, 1998). As can be seen in Eq. (1), when $s$ is less than 1, $\Psi(\eta)$ corresponds to a high-frequency function; when $s$ is greater than 1, $\Psi(\eta)$ corresponds to a low-frequency function.

The wavelet coefficients ($W_\Psi$) of CWT for the time series $x_t$ (with equal time interval, $\delta t$), is calculated using the convolution of $x_t$ with the scaled and translated versions of the wavelet, $\Psi(\eta)$ (Partal and Küçük, 2006):

$$W_\Psi(s,\gamma) = \frac{1}{\sqrt{s}}\int_{-\infty}^{\infty} x(t)\Psi^*\left(\frac{t-\gamma}{s}\right)\delta t \tag{2}$$

where the asterisk symbol represents the complex conjugate numbers. If the scale ($s$) and translation ($\gamma$) functions are smoothly changed according to time $t$, a scalogram can be produced from the calculation, revealing the amplitude of a specific scale and how it fluctuates over time (Torrence and Compo, 1998).

#### 2.1.2. Discrete Wavelet Transform (DWT)

Although CWT is able to locate specific events in a signal that may not be obvious, one of the main disadvantages of the CWT is that the construction of the CWT inverse is more complicated (Fugal, 2009). In practice this may not always be desirable because often, signal reconstructions are needed (Fugal, 2009). In addition, the use of the CWT can generate too many data (coefficients) and is more difficult to implement. It may also be more desirable to choose the DWT over CWT because CWT does not produce information in the form of a time series, but rather in a two-dimensional format (Percival, 2008). This causes a high amount of redundant information produced by CWT and the coefficients are correlated spatially and temporally (Percival, 2008). If the DWT is chosen, the process of transformation is simplified and the amount of work is reduced; yet, it still produces a very efficient and accurate analysis (Partal and Küçük, 2006). This is because the DWT is normally based on the dyadic calculation of position and scale of a signal (Chou, 2007). The DWT of a vector is the outcome of a linear transformation resulting in a new vector that has equal dimensions to those of the initial vector (Chou, 2011). This transformation is the decomposition process. The discretization of wavelet functions is accomplished using a logarithmic uniform spacing that has a coarser resolution at higher scales (Mallat, 1989; Daubechies, 1990).

Some important features of DWT are: (i) at each scale, the number of convolutions using orthogonal wavelets is proportional to the width of the wavelet function at that particular scale (Torrence and Compo, 1998; Kulkarni, 2000); (ii) the wavelet spectra generated are in discrete steps and give a very compact representation of the signal (Kulkarni, 2000); (iii) due to its orthogonal property, signal reconstruction is not complicated (Torrence and Compo, 1998); and (iv) results of transformations using DWT do not contain the unwanted relation between the wavelet coefficients, which are observed in the CWT (i.e. DWT removes the redundant information within the wavelet coefficients in order to better identify processes contained in signals) (Daubechies, 1992). DWT adopts the following form (Partal and Küçük, 2006):

$$\Psi_{(a,b)}\left(\frac{t-\gamma}{s}\right) = \frac{1}{(s_0)^{a/2}}\Psi\left(\frac{t-b\gamma_0 s_0^a}{s_0^a}\right) \tag{3}$$

$\Psi$ denotes the mother wavelet; $a$ and $b$ are integers, which represents the amount of dilation (scale factor) and translation of the wavelet, respectively; $s_0$ denotes a dilation step whose value is unchanged and is greater than 1; and $\gamma_0$ symbolizes the location variable whose value is greater than zero. Generally, for practical reasons, the values for $s_0$ and $\gamma_0$ are chosen to be 2 and 1, respectively (Mallat, 1989; Daubechies, 1992). This is the DWT dyadic grid arrangement (i.e. integer powers of two; logarithmic scaling of the translations and dilations). If a time series exhibits discrete properties, with a value of $x_t$, occurring at a discrete time $t$, the wavelet coefficient ($W_\psi(a,b)$) for the DWT becomes (Partal and Küçük, 2006):

$$W_\psi(a,b) = \frac{1}{(2)^{\frac{a}{2}}}\sum_{t=0}^{N-1} x_t \Psi\left(\frac{t}{2^a} - b\right) \tag{4}$$

The wavelet coefficient for the DWT is calculated at scale $s = 2^a$ and location $\gamma = 2^a b$, revealing the variation of signals at different scales and locations (Partal and Küçük, 2006). Since most precipitation and streamflow data are sampled in discrete intervals, it makes sense to use the DWT.

### 2.2. The Mann–Kendall (MK) trend test

The computation of the MK $S$-statistic value from the raw data can yield a large positive or negative value for $S$, indicating a positive or negative trend, respectively. The null hypothesis ($H_o$) of the MK test assumes that the ranked data ($X_c$, $c = 1, 2, 3, \ldots, n-1$) and ($X_d$, $d = c+1, \ldots, n$) belong to a sample of $n$ independent and identically distributed random variables. The alternative hypothesis ($H_1$) of the two-sided test assumes that the distributions of $X_c$ and $X_d$ are not identical for all $c$, $d \leqslant n$ with $c \neq d$ (Partal, 2010). The $S$-statistic of the MK test is computed as (Hirsch and Slack, 1984):

$$S_t = \sum_{c=1}^{n-1}\sum_{d=c+1}^{n} sign(X_d - X_c) \tag{5}$$

$$Sign(X_d - X_c) = \begin{cases} +1, & when\ X_d > X_c \\ 0, & when\ X_d = X_c \\ -1, & when\ X_d < X_c \end{cases} \tag{6}$$

$X_c$ and $X_d$ denote the ranked values of the data, and $n$ is the length of the data record. For data that are distributed identically and independently with a zero mean, the variance for the $S_t$ statistic can be calculated as (Adamowski and Bougadis, 2003):

$$Variance(S_t) = \left\{ n(n-1)(2n+5) - \sum_{c=1}^{n} t_c(c)(c-1)(2c+5) \right\} \Big/ 18 \tag{7}$$

$t_c$ represents the summation of $t$, which is the number of tied values to the extent of $c$. The statistic of the Mann–Kendall test, $Z$, is then given as (Xu et al., 2009):

$$Z = \begin{cases} \frac{S_t - 1}{\sqrt{Variance(S_t)}}, & (if\ S_t > 0) \\ 0, & (if\ S_t = 0) \\ \frac{S_t + 1}{\sqrt{Variance(S_t)}}, & (if\ S_t < 0) \end{cases} \tag{8}$$

The statistic of the MK test, $Z$, given in Eq. (8) can be used where the number of records, $n$, is larger than 10. The trend's significance is assessed by comparing the $Z$ value with the standard normal variate at the pre-specified level of statistical significance (Hamed and Rao, 1998). In a two-sided trend test, with alpha ($\alpha$) representing the significance level, the null hypothesis should not be accepted if $|Z| > Z_{\alpha/2}$; this suggests that the trend is significant. A positive $Z$-value at the significance level implies that there is a positive trend, whereas a negative value indicates a negative trend. The probability value ($p$-value) obtained from the MK $Z$-value can be used to verify the significance of a trend. If the $p$-value is less than the pre-determined significant level (e.g. $\alpha = 5\%$) or greater than the confidence level (if $\alpha = 5\%$, confidence level = 95%), it means that the null hypothesis of no trend cannot be accepted.

#### 2.2.1. Modified Mann–Kendall (MK) trend tests that account for seasonality and autocorrelation structures in the data

It is well known that the original Mann–Kendall test does not consider the autocorrelation factor that may be present in the time series being analyzed. The presence of an autocorrelation in a dataset may lead to inaccurate interpretations of the MK test. A time series exhibiting positive autocorrelation causes the effective sample size to be less than the actual sample size, thereby increasing the variance and the possibility of detecting significant trends when in fact, there are no trends (Hamed and Rao, 1998; Ehsan-

zadeh et al., 2011). On the contrary, the existence of negative autocorrelation in a time series enhances the possibility of accepting the null hypothesis (absence of significant trends), when actually, there are significant trends (Ehsanzadeh et al., 2011).

There have been several approaches developed that deal with the effects of autocorrelation in a time series. Yue et al. (2002) developed the Trend-Free Pre-whitening method (TFPW) – the trend component is assumed to be linear, and is first removed before the pre-whitening procedure is applied. Kumar et al. (2009) found that for data that have significant autocorrelation coefficients extending beyond the first lag, the TFPW method was not the best method to account for all these significant autocorrelations. In the present study, significant autocorrelations may be present for more than just one lag in several time series. Therefore, the TFPW method is not considered in this study.

Hirsch and Slack (1984) proposed a modified MK test that accounts for seasonality and serial dependence factors. This method separates observations into different seasons, which eliminates the dependence problem between seasons (Hirsch et al., 1982; Hirsch and Slack, 1984). This method, however, is not as powerful when there is long-term persistence (with autoregressive parameter > 0.6) or when there are less than 5 years worth of monthly data (Hirsch and Slack, 1984).

Hamed and Rao (1998) proposed another modified version of the MK test in order to deal with the issue of autocorrelation structures for all lags in a dataset, because autocorrelations may still exist past the first lag (note: seasonality issues are not taken into consideration in this modified version of the MK test). Since the presence of autocorrelation underestimates the variance if calculated using the MK formula for uncorrelated data, the method by Hamed and Rao (1998) modifies the calculation for the variance of the MK test statistics when the data are serially correlated by using an empirical formula (see Section 2.2.3). When applied to autocorrelated data with a large sample size, this test was found to be practically as powerful as when the original MK test is applied to independent data (Hamed and Rao, 1998).

*2.2.2. Modified Mann–Kendall (MK) test to account for seasonality and autocorrelation by Hirsch and Slack (1984)*

Hirsch and Slack (1984) modified the original Mann–Kendall trend test to account for seasonality and autocorrelation factors present in a dataset. Let the matrix:

$$x = \begin{pmatrix} x_{11} & x_{12} & x_{13} & \dots & x_{1k} \\ x_{21} & x_{22} & x_{23} & \dots & x_{2k} \\ x_{31} & x_{32} & x_{33} & \dots & x_{3k} \\ \vdots & \vdots & \vdots & & \vdots \\ x_{j1} & x_{j2} & x_{j3} & \dots & x_{jk} \end{pmatrix} \tag{9}$$

where the data in the matrix $x$ represent a series of observations recorded over $k$ seasons for $j$ years (without any tied values) (Hirsch and Slack, 1984). The ranks of the data in matrix $x$ are represented in the following matrix (Hirsch and Slack, 1984):

$$r = \begin{pmatrix} r_{11} & r_{12} & r_{13} & \dots & r_{1k} \\ r_{21} & r_{22} & r_{23} & \dots & r_{2k} \\ r_{31} & r_{32} & r_{33} & \dots & r_{3k} \\ \vdots & \vdots & \vdots & & \vdots \\ r_{j1} & r_{j2} & r_{j3} & \dots & r_{jk} \end{pmatrix} \tag{10}$$

Since the values within each season are ranked among themselves, the calculation of the rank ($r_{dz}$) becomes (Hirsch and Slack, 1984) (for $c$ and $d$ notations, see Eq. (5)):

$$r_{dz} = \frac{[j + 1 + \sum_{c=1}^{j} sgn(x_{dz} - x_{cz})]}{2} \tag{11}$$

The test statistic $S_z$ is calculated using (for each season):

$$S_z = \sum_{c<d} sgn(x_{dz} - x_{cz}); \quad where\ z = 1, 2, 3, \dots k \tag{12}$$

The test statistics for the seasonal Kendall is calculated using:

$$S_s = \sum_{z=1}^{k} S_z \tag{13}$$

with variance of:

$$Variance\ S_s = \sum_{z} (\sigma_z)^2 + \sum_{z,w;z\neq w} \sigma_{zw} \tag{14}$$

$\sigma_z^2$ is the variance of ($S_z$), $\sigma_{zw}$ denotes the covariance of ($S_z$,$S_w$). The estimator for the covariance $\hat{\sigma}_{zw}$ was developed by Dietz and Killeen (1981), which is as follows:

$$\hat{\sigma}_{zw} = \frac{K_{zw}}{3} + (j^3 - j)\frac{r^*_{zw}}{9} \tag{15}$$

With no missing values, the estimator of the covariance becomes (Hirsch and Slack, 1984):

$$\hat{\sigma}_{zw} \frac{\left(K_{zw} + 4\sum_{c=1}^{j} r_{cz} r_{cw} - j(j+1)^2\right)}{3} \tag{16}$$

where $K_{zw}$ and $r^*_{zw}$ are calculated using:

$$K_{zw} = \sum_{c<d} sgn((X_{dj} - X_{cj})(X_{dw} - X_{cw})) \tag{17}$$

$$r^*_{zw} = \left(3/(j^3 - j)\right) \sum_{c,d,p} sgn(X_{dj} - X_{cj})(X_{dw} - X_{pw}) \tag{18}$$

However, in the event that there are no ties and no missing data values, $r^*_{zw}$ is simply the Spearman's correlation coefficient for seasons $z$ and $w$ (Hirsch and Slack, 1984). By adopting the estimates of $\sigma_{zw}$ to calculate the variance $S_s$, the test no longer needs the assumption of independence (Hirsch and Slack, 1984).

*2.2.3. Modified Mann–Kendall test for autocorrelated data by Hamed and Rao (1998)*

Since using the original MK for autocorrelated data underestimates the variance of the data, the calculation of the variance of the test statistics $S$ is altered and given by an empirical formula (Hamed and Rao, 1998):

$$Variance\ (S') = (n(n-1)(2n+5)/18) \cdot \left(\frac{n}{n^*_e}\right) \tag{19}$$

where $n^*$ is the effective number of sample size needed in order to account for the autocorrelation factor in the dataset. The notation $n/n^*_e$ is the factor that represents the correction associated with the autocorrelation of the data. Empirically, the correction is expressed by Hamed and Rao (1998):

$$\frac{n}{n^*_e} = 1 + \left(\frac{2}{n^3 - 3n^2 + 2n}\right) \cdot \sum_{f=1}^{n-1} (n-f)(n-f-1)(n-f-2)\rho_e(f) \tag{20}$$

$\rho_e(f)$ symbolizes the autocorrelation function between the ranks of the observations, computed using the inverse of Eq. (19) (Kendall, 1975; Hamed and Rao, 1998). This transforms the rank autocorrelation into the normalized data autocorrelation, as the estimate of the normalized autocorrelation structure is needed to evaluate the variance of $S$ for data $X$ whose distribution may not be normal or rather arbitrary (Hamed and Rao, 1998).

$$\rho(f) = 2\sin\left(\frac{\pi}{6}\rho_e(f)\right) \quad (21)$$

## 3. Study sites and datasets

The monthly, seasonally-based and annual flow and precipitation data from a total of eight Reference Hydrometric Basin Network (RHBN) stations and seven meteorological stations, respectively, were analyzed. These stations are located in Ontario and Quebec, Canada. Six of the RHBN stations used are located in Ontario, and two are in Quebec. The smallest drainage area of the flow stations is 181 km$^2$ and the largest one is 22,000 km$^2$. As for the meteorological stations, there are three situated in Quebec, and one in Ontario. The two Quebec RHBN stations – Richelieu River and Eaton River – are located in the south western corner of the province, on the south shore portion of the St. Lawrence stream. Four RHBN stations in Ontario (the Neebing, North Magnetawan, Black, and Sydenham rivers) are located around the Great Lakes basin. The Missinaibi and Nagagami rivers (Ontario) are the most northerly stations. The locations of the flow and precipitation stations are shown in Fig. 1 and the key features of the RHBN stations and the meteorological stations are summarized in Tables 1 and 2, respectively.

Monthly datasets were chosen because it includes the analysis of short-term monthly variations such as the intra-annual and inter-annual cycles. Seasonally-based values were examined to allow the analysis of seasonal cycles (it will be seen later that most time series – especially flow time series – exhibit strong annual cycles). Annual datasets were analyzed in order to study the long-term fluctuations (e.g. multi-year, decadal, and multi-decadal events) that are potentially present in the flow and precipitation time series.

One of the advantages in using monthly datasets compared to annual datasets in trend detection is that annual data values may not deal well with the presence of missing records (which causes the annual summary value to be biased), and the seasonality factor (Hirsch and Slack, 1984). If both factors (missing data and seasonality) are present in a yearly time series, the trends detected may simply be caused by the yearly variation in the sampling schedule (Hirsch and Slack, 1984). Having said this, a monthly time series has more autocorrelation issues compared to a yearly time series (Hirsch and Slack, 1984). Therefore, this present study chose to incorporate monthly and annual data in order to thoroughly analyze the variations and trends of flow and precipitation within the study area.

### 3.1. Selection criteria for the RHBN flow stations and meteorological stations

The stations used in this study were chosen based on the regulation type (for flow stations), and the completeness and length of their available records for the period of 1954–2008. The three main criteria used for this selection are summarized as follows: (1) there must be an absence of hydrological structural controls upstream of a RHBN gauging station (for flow stations only). Upstream controls and regulation, such as reservoir storage or containment structures, hydropower activities, and water diversions may have considerable impacts on the quality of data (Yue and Pilon, 2005). As a consequence, less accurate frequency analysis and interpretation may be obtained. Therefore, this study only considered gauging stations, which are stated as "natural" according to Environment Canada. (2) Stations must have a record length of at least 55 years, starting from 1954 to 2008. In order to obtain a valid mean statistic in assessing trends in flow associated with climate change, Kahya and Kalayci (2004) and Burn and Hag Elnur (2002) consider that at least 31 and 25 years worth of data, respectively, are required. Furthermore, Partal (2010) considered 40 years' worth of data adequate for trend analysis studies. Therefore, we concluded that having 55 years worth of data would be sufficient for the purpose of trend detection in our study. The start and end years in this study were chosen because they would give the highest number of stations in Quebec and Ontario to be analyzed without any missing

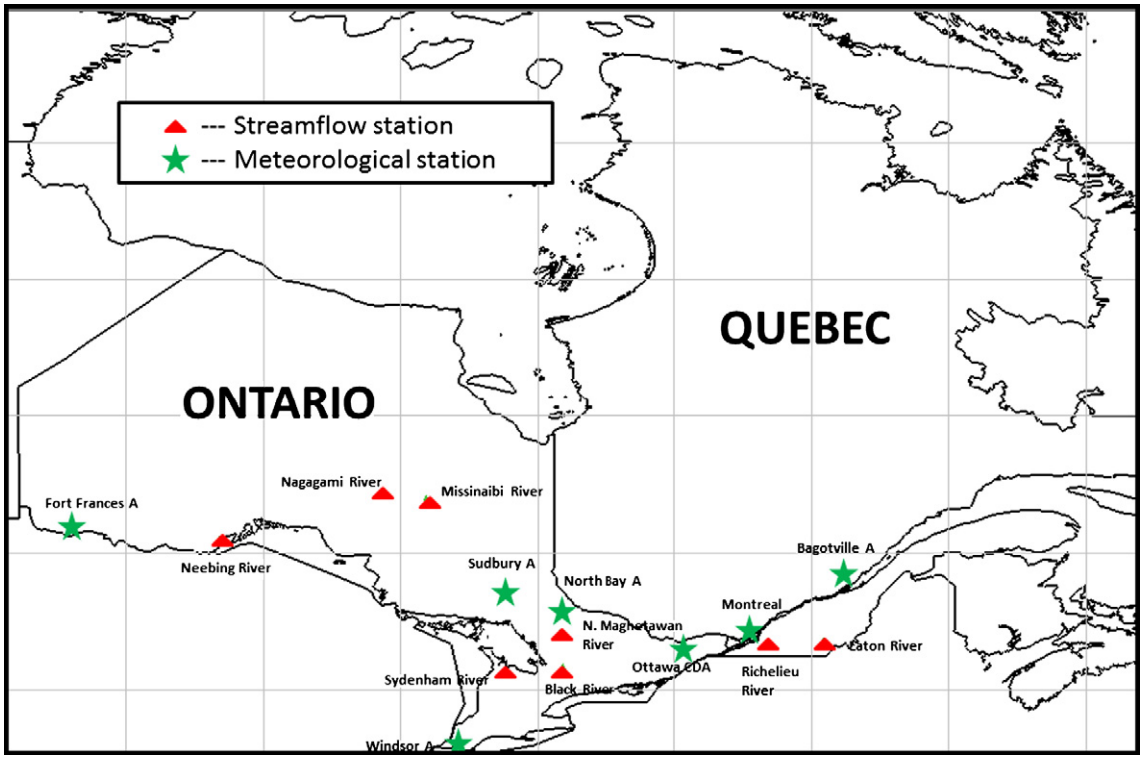


**Fig. 1.** A map of the flow and precipitation stations used this study.

**Table 1**
Unregulated RHBN gauging stations in Ontario and Quebec recording the streamflow data, which were used in this study.

| Station Id. | Station name | Province | Latitude (°) | Longitude (°) | Drainage area (km$^2$) |
|---|---|---|---|---|---|
| 02AB008 | Neebing River near Thunderbay | ON | 48.38 | −89.31 | 187 |
| 02EA005 | North Magnetawan River Near Burk's Falls | ON | 45.66 | −79.37 | 321 |
| 02EC002 | Black River Near Washago | ON | 44.71 | −79.28 | 1521 |
| 02FB007 | Sydenham River Near Owen Sound | ON | 44.52 | −80.93 | 181 |
| 02OE027 | Eaton (Riviere) Pres De La Riviere Saint-Francois-3 | QC | 45.46 | −71.65 | 642 |
| 02OJ007 | Richelieu (Riviere) Aux Rapides Fryers | QC | 45.39 | −73.25 | 22,000 |
| 04JC002 | Nagagami River At Highway No. 11 | ON | 49.77 | −84.53 | 2410 |
| 04LJ001 | Missinaibi River At Mattice | ON | 49.61 | −83.26 | 8940 |

**Table 2**
Meteorological stations in Ontario and Quebec recording the precipitation data, which were used in this study.

| Station id. | Station name | Province | Latitude (°) | Longitude (°) | Joint station | Elevation (m) |
|---|---|---|---|---|---|---|
| 6022476 | Fort Frances A | ON | 48.7 | −93.43 | Yes | 342 |
| 6068150 | Sudbury A | ON | 46.6 | −80.8 | Yes | 348 |
| 6085700 | North Bay A | ON | 46.4 | −79.4 | Yes | 370 |
| 6105976 | Ottawa CDA | ON | 45.4 | −75.7 | No | 79 |
| 6139525 | Windsor A | ON | 42.3 | −82.9 | Yes | 190 |
| 7025250 | Montreal/Pierre Elliot Trudeau Intl. A | QC | 45.5 | −73.8 | Yes | 36 |
| 7060400 | Bagotville A | QC | 48.33 | −71 | No | 159 |

records. (3) Although up to three-percent missing data is considered acceptable for meteorological studies (Mishra and Singh, 2010), this study chose to include only stations with fully complete records over the chosen time period. This was done in order to avoid possible uncertainties associated with the computation of extrapolation procedures. Criterion number 1 was applied only to the flow stations; criteria number 2 and 3 were applied to both flow and precipitation stations. In summary, there are a total of eight RHBN stations in Ontario and Quebec that meet the three selection criteria. As for the meteorological stations, there are a total of seven meteorological stations in Ontario and Quebec that have a record length of 55 years without missing values.

### 3.2. Flow data

The monthly, seasonal, and annual average flow data were obtained from the Environment Canada HYDAT database. Only data from stations that are categorized as RHBN were chosen. First, the RHBN designation for a station indicates that its data accuracy is further evaluated qualitatively by local experts by taking into consideration the hydraulic condition of that particular station (Coulibaly and Burn, 2004). Secondly, the stage–discharge relationship and channel geometry were considered, and the reliability of data records influenced by ice conditions was checked (Zhang et al., 2001). Thirdly, the RHBN stations represent pristine or stable hydrological conditions, having at least 20 years of good-quality data (Zhang et al., 2001). In summary, only RHBN gauging stations were included in this study in order to ensure that good-quality data are used. In addition to this, many Canadian studies on flow trend and variability have also used data from selected RHBN stations because of their record length and reliability (e.g. Burn and Hag Elnur, 2002; Coulibaly and Burn, 2004; Ehsanzadeh and Adamowski, 2007; Ehsanzadeh et al., 2011, etc.).

The flow data used in this study cover the period from January 1954 to December 2008, except for Eaton River station that has records ending in September 2008. The data analysis therefore covers the years 1954–2008 (except for Eaton River which only covers up to 2007 due to the incomplete 2008 data).

### 3.3. Precipitation data

The monthly, seasonally-based and annual total precipitation data were obtained from Environment Canada's second generation adjusted and homogenized precipitation data base (with trace corrections to account for trace amounts of both rainfall and snowfall). The detailed explanation of the adjustment procedures can be found in Mekis and Vincent (2011). Daily rainfall and snowfall measurements were adjusted separately – the adjusted rainfall and snow-water equivalent make up the daily total precipitation (Mekis and Vincent, 2011). Mekis and Vincent (2011) also applied several statistical adjustments to the original daily data (which were taken from the National Climate Data Archive of Environment Canada). These procedures address issues regarding changes in location, modifications to recording instruments, faulty equipment, and alterations to recording procedures. These corrections were done to ensure that factors such as wind undercatch, evaporation losses, and gauge specific wetting losses for specific types of rain-measuring instruments, have been taken into account. Other improvements and revisions that were also implemented by Mekis and Vincent (2011) in these second generation datasets include: better rain-gauge adjustment procedures, improved snow-water equivalent maps, better adjustment procedures to trace records due to more accurate metadata information, and further tests on the combined stations. Since the datasets contained in the second generation adjusted precipitation data have been developed mainly for climate-related research, their quality is very suitable for the purpose of this study.

Many precipitation stations included in the second-generation datasets have long records as a result of data combinations among nearby stations (Mekis and Vincent, 2011). The procedures and adjustments involved in joining the data of nearby stations are given in detail in Mekis and Vincent (2011). The stations used in this study were combined stations, except for the Ottawa CDA and Bagotville A stations (Table 2). All precipitation stations used have data that extend prior to 1954. Station Sudbury A has incomplete data for year 2008; therefore the data analysis for this station only covers up until 2007. To be consistent with the analysis of the flow trends, it was decided to use the common period of 1954–2008. Kumar et al. (2009) suggested that the same length of records should be used when analyzing trends of different variables to avoid misleading conclusions.

## 4. Methodology

Three data types were used in the data analysis: monthly, seasonally-based, and annual. Monthly time series allowed for the

investigation of the short-term fluctuations that affect the flow and precipitation. Since annual cycles were strongly apparent in most monthly data, the seasonal average flow and the seasonal total precipitation were used to assess if these annual cycles may have an influence on trends in flow and precipitation data – the second decomposition level in the seasonally-based data represented the yearly (12-month) cycle. Finally, annual data were used in order to assess the long-term fluctuations of streamflow and precipitation over the study area.

The procedures for data analysis are organized in the following order:

1. Autocorrelation tests or analysis were performed for each of the precipitation and streamflow series in order to check for the presence of a serial correlation and seasonality patterns.
2. Each time series was decomposed via the Discrete Wavelet Transform (DWT) using Daubechies wavelets, splitting the signal into its approximation and detail components.
3. The Mann–Kendall tests were computed on the original data, the detail time series, as well as on the combinations of each of the detail components plus their approximations.
4. The sequential Mann–Kendall analysis was applied to every time series, starting from the original series to the different detail components, approximations, and the combinations of the details with their approximations.
5. The periodic component(s) responsible for trends in each dataset were determined based upon the MK $Z$-values and the sequential MK graphs of each periodicity.

The sequential MK graphs of the original annual time series were analyzed and used to determine the starting point of a trend increase or decrease. This was done in order to examine whether these starting times are similar among the different flow and precipitation stations. The following sections describe each of these steps in detail.

### 4.1. Autocorrelation analysis

The presence of significant autocorrelation in a time series can compromise the interpretation of its trend analysis because it can alter the dispersion of the data distribution by changing the variance. This then increases the occurrence of type I error (Yue et al., 2002), in which a significant trend may be found when in fact the null hypothesis should be accepted (Hamed and Rao, 1998; Partal, 2010). It is expected that the monthly and seasonally-based data would have more autocorrelation issues compared to the annual data. An autocorrelation assessment in the monthly and seasonal datasets was accomplished by using the following equation (Yue et al., 2002; Mohsin and Gough, 2010):

$$R = \frac{(1/n-1)\sum_{t=1}^{n-1}[x_t - \bar{x}_t][x_{t+1} - \bar{x}_t]}{(1/n)\sum_{t=1}^{n}[x_t - \bar{x}_t]^2} \tag{22}$$

$$\frac{\{-1 - 1.645\sqrt{n-2}\}}{n-1} \leqslant R \leqslant \frac{\{-1 + 1.645\sqrt{n-1}\}}{n-1} \tag{23}$$

$R$ is the lag-1 autocorrelation coefficient of the sample data $x_t, \bar{x}_t$ is the sample mean, and $n$ is the number of observations in the data. If the calculated lag-1 autocorrelation coefficient is within the interval defined by Eq. (23), it can be assumed that the monthly or seasonal dataset does not contain a significant autocorrelation. If, on the other hand, the calculated $R$ is found to be outside of the range, the corresponding dataset is assumed to exhibit a significant autocorrelation at the 5% significance level. For the annual datasets, their correlograms showing the ACFs of each dataset for several lags were analyzed and used to determine whether the data are autocorrelated.

### 4.2. Seasonality factor

The monthly and seasonally-based flow and precipitation time series were checked for seasonality by examining their correlograms. These correlograms were used to visually determine the presence (or lack thereof) of seasonality patterns, or of any cyclical and oscillatory behavior. Looking at the original data, many time series display the patterns of significant autocorrelation and annual cycles. It is important to note that the detail components of signal decomposition in WT can be associated with factors such as seasonal cycles, and other influencing variables that may be external to the time series (Choi et al., 2011). Therefore, the correlograms of the detail components were used to check whether any cyclical patterns were still present post-decomposition.

### 4.3. Time series decomposition via the Discrete Wavelet Transform (DWT)

The conventional discrete wavelet analysis of signals was performed on each flow and precipitation time series using the *multilevel 1-D wavelet decomposition* function in MATLAB (MATLAB Wavelet Toolbox). This produces the wavelet transform of the input data at all dyadic scales. Rather than relying on an upsampling procedure, the DWT relies more on downsampling, which is excellent for denoising (Fugal, 2009). The mean flow and total precipitation input signals (data) are all one-dimensional.

Decomposing the signals using specified filters (wavelet and scaling functions) produces two types of coefficients: the approximation or residual, and detail vectors (Chou, 2007). These coefficients resulted from the convolution of the original signal with a low-pass filter and a high-pass filter. The low-pass filter is the scaling function and the high-pass filter is the wavelet function. The convolutions of signals with the low-pass filter produced the approximation coefficients, which represent the large-scale or low-frequency components of the original signal. Convolutions with the high-pass filter produced the detail coefficients, which represent the low-scale or high-frequency components (Bruce et al., 2002). The process of signal decomposition was repeated multiple times, decomposing the original signal into several different lower-resolution components (Partal, 2010).

The detail and approximation coefficients produced from the signal decomposition were then reconstructed since they are merely intermediate coefficients. These have to be re-adjusted to the entire one-dimensional signal in order to enable the investigation of their contribution to the original signal (Dong et al., 2008). This contribution may be reflected in the different time scales such as intra-annual, inter-annual, decadal, and multi-decadal.

The Daubechies (db) wavelets were used in this study because they are commonly used mother wavelets for the DWT in hydrometeorological wavelet-based studies. Daubechies wavelets provide compact support (Vonesch et al., 2007), indicating that the wavelets have non-zero basis functions over a finite interval, as well as full scaling and translational orthonormality properties (Popivanov and Miller, 2002; de Artigas et al., 2006). These features are very important for localizing events in the time-dependent signals (Popivanov and Miller, 2002).

Relatively large numbers of data points used in this study were from the monthly and seasonally-based datasets. For the period of 55 years, there were 657 or 660 data points for the monthly sets and 219 or 220 for the seasonally-based sets, depending on when the records ended in 2008. In order to avoid unnecessary levels of data decomposition in these larger datasets, the number of decomposition levels had to be determined first. This number is based upon

the number of data points, as well as the mother wavelet used. The highest decomposition level should correspond to the data point at which the last subsampling becomes smaller than the filter length (de Artigas et al., 2006). According to de Artigas et al. (2006), who analyzed monthly geomagnetic activity indices, if $v$ is the number of vanishing moments of a db wavelet and $n$ is the number of data points in a monthly-based time series, the maximum decomposition level $L$ is calculated using the following equation:

$$L = \frac{Log\left(\frac{n}{2v-1}\right)}{Log(2)} \tag{24}$$

In MATLAB, the number of vanishing moments for a db wavelet is half of its starting filter length. For example, db5 in MATLAB refers to the Daubechies5 wavelet, which has a 10-point filter length. If one uses db5 to analyze the monthly data, for example, in Eq. (24), with $v$ equal to 5, the resulting maximum level of decomposition for the monthly data is 6.20 (the DWT performed in MATLAB would consider the data up to the next dyadic arrangement, which is 1024 data points instead of 660).

Smoother db wavelets (db5–db10) were then tried for each monthly and seasonally-based dataset. Smoother wavelets are preferred here because the trends are supposed to be gradual and represent slowly-changing processes. Smoother wavelets should be better at detecting long-term time-varying behavior (good frequency-localization properties) (Adamowski et al., 2009). In addition to this, several trend studies used smoother db mother wavelets (e.g. Kallache et al., 2005 used *least asymmetric* LA (8); de Artigas et al., 2006 used db7). With the smoother db wavelets, the levels of decomposition resulting from the calculations using Eq. (24) were between 5.8 and 6.8 (for monthly-based data), and 3.8 and 4.8 (for seasonally-based data). Therefore, six and seven levels; and four and five levels were tried for the monthly and seasonally-based data, respectively.

The border conditions were also taken into consideration when performing the DWT. This is because for signals with a limited length, convolution processes cannot proceed at both ends of the signal since there is no information available outside these boundaries (Su et al., 2011). This is referred to as the border effect (Su et al., 2011). As a result, an extension at both edges is needed. Border extensions that are commonly used are zero-padding, periodic extension, and symmetrization – all of which have their drawbacks, due to the discontinuities introduced at both ends of the signals (de Artigas et al., 2006; Su et al., 2011). The default extension method used in MATLAB is symmetrization, which assumes that signals outside the original support can be recovered by symmetric boundary replication (de Artigas et al., 2006). Zero-padding pads the signal with zeros beyond the original support of the wavelet; periodic padding assumes that signals can be recovered outside of the original support by periodic extension (de Artigas et al., 2006). The Inverse Discrete Wavelet Transform (IDWT) was then computed to ensure perfect signal reconstruction.

For each monthly dataset, six and seven levels of decomposition were tried for each smooth db wavelet. In order to determine the smooth mother wavelet and the extension mode to be used in the data analysis for each data type and dataset, two criteria were used. The first criterion used was proposed by de Artigas et al. (2006): all three extension modes for each db wavelet were employed in order to determine the extension method, and the db type, that would produce the lowest mean relative error *(MRE)*. The mean relative error (*MRE*) was calculated using the following equation (Popivanov and Miller, 2002; de Artigas et al., 2006):

$$MRE = 1/n\sum_{j=1}^{n}\frac{|a_j - x_j|}{|x_j|} \tag{25}$$

where $x_j$ is the original data value of a signal whose number of records is $n$, and $a_j$ is the approximation value of $x_j$. The second criterion is the one proposed in this study and is based on the relative error ($e_r$). Each of the extension modes for each of the smooth db wavelets was examined in order to determine the combination (of border condition and the mother wavelet) that would produce the lowest approximation Mann–Kendall $Z$-value relative error ($e_r$). The computation of the relative error was done using the following proposed equation:

$$e_r = \frac{|Z_a - Z_o|}{|Z_o|} \tag{26}$$

where $Z_a$ is the MK $Z$-value of the last approximation for the decomposition level used, and $Z_o$ is the MK $Z$-value of the original data.

For the monthly datasets, the calculated *MREs* did not differ significantly among the different border conditions and the different db wavelet types used, for the six and seven levels of decomposition. However, once the $e_r$ calculations were completed, the lowest errors were generally obtained for six decomposition levels. Therefore, for the monthly data analysis, six decomposition levels were used in their DWT procedures (the db type and border extensions may vary from one station to another). The $e_r$ was then used to determine the db type as well as the border extension to be used for the data analysis. Using the monthly total precipitation for station Montreal/Pierre Elliot Trudeau as an example, the *MREs* for the different db types and border extensions were between 0.42 and 0.43 (this applied both for six and seven decomposition levels). The ranges of the $e_r$ for six decomposition levels were: 97.35–341.05, 44.78–421.94, and 17.46–134.65 using zero-padding, periodic extension, and symmetrization borders, respectively. As can be seen, there were very noticeable differences in the relative errors among the different extensions. For this station, the lowest $e_r$ produced was by using the symmetrization border with db9 ($e_r$: 17.46, *MRE*: 0.42).

For the seasonally-based data analysis, similar procedures to that of the monthly data analysis were used, in order to find the levels of decomposition, db type, and border extension that would produce the lowest *MRE* and $e_r$. Four and five levels of decomposition were tried with different border conditions for the different smooth db wavelets. The lowest *MRE* and $e_r$ were obtained when four levels of decomposition were used. Therefore, four levels of decompositions were used for the seasonally-based data analysis, but the extensions and db types may vary for the different stations.

For the annual data, similar observations were seen where the *MREs* of the different border conditions did not show substantial differences. The differences in the relative errors were also more noticeable among the different border extensions and the different db wavelets. Since the annual datasets have 55 years worth of records, they could be decomposed up to five levels, which correspond to 32 years. Even so, four decomposition levels – which have a maximum of 16 years in fluctuation – were also explored. The $e_r$ and *MRE* of four decomposition levels were then compared to those of five decomposition levels. So, four and five levels of decompositions were assessed for the annual data. The *MREs* between the two levels did not produce significant differences, but lower relative errors were observed for four decomposition levels. For example, for the North Magnetawan River station, the *MREs* for levels four and five were 0.17–0.22 and 0.17–0.25, respectively. The lowest relative errors for this station were observed when the periodic border extension was used at four decomposition levels with different db types ($e_r$ = 0.98–4.97). Therefore, for this station, four decomposition levels were used in the DWTs, with the periodic extension border and db10 wavelet – this produced the lowest relative error (i.e. 0.98). The same procedures were applied to the rest of the annual datasets – four decomposition levels were used, but the extension condition and db wavelet types may vary from one station to another.

### 4.4. Applying the Mann–Kendall (MK) trend tests

For each study location, the MK test *S*-statistic and its variance were calculated in order to obtain the test's *Z* standard normal value. The absolute value of this *Z*-value was then compared to the critical two-tailed *Z*-value (area under the normal curve) corresponding to the significant level of $\alpha/2$ (this study used $\alpha = 5\%$). The *Z* values in a two-tailed test for $\alpha$ of 5% are ±1.96. If the *Z*-value obtained from the MK calculation is found outside the boundary of −1.96 and +1.96, then that indicates that the trends detected are significant.

For the monthly and seasonally-based datasets, the modified MK test by Hirsch and Slack (1984) was used because all of these time series showed seasonality patterns and most of them exhibited significant lag-1 autocorrelations. For the annual datasets, the original MK test was applied to datasets that did not exhibit significant autocorrelation. The modified MK test by Hamed and Rao (1998) was applied to two annual datasets (Richelieu River and Montreal/Pierre Elliot Trudeau) because they possessed significant autocorrelations. These corresponding MK tests for the different data types were computed on the original time series, the time series resulting from the wavelet decomposition (details and approximations), and on a set of combinations of the details plus their respective approximations.

### 4.5. Sequential Mann–Kendall (MK) analysis

The progressive MK values were calculated for the data used ranging from the beginning of the study period to the end (e.g. Partal, 2010). These MK values were obtained using the different MK tests for the different data characteristics (mentioned in Section 4.4). The MK values were portrayed as line graphs and when the line crosses the upper or lower confidence limits, it is an indication that there is a significant trend because the calculated MK value is greater than the absolute value of the normal standard *Z* value (at the 5% significance level). By using this significance level, it is implied that the upper confidence limits in a sequential MK graph represent the *Z*-value of +1.96, whereas the lower confidence limits represent the *Z*-value of −1.96. The purpose of conducting the sequential MK tests and graphing the results is to see how the trends fluctuated over the study period. Sequential MK analysis also allowed the depiction of a combination of a set of significant upward and downward trends in a time series that may cancel each other, resulting in a non-significant final MK *Z*-value for that specific dataset.

It is important to note that the normal approximation may be used on the MK test to obtain the *Z*-value only when the number of data points is greater than 10. Additionally, the power of the modified MK test by Hirsch and Slack (1984) is considered acceptable when seasonal datasets have at least 10 years worth of monthly values. In light of this, the present study considered the MK values to be accurate starting from the 10th year since the beginning of the data record, which is 1963. Although all of the sequential MK graphs presented in this paper cover the entire study period from 1954 to 2008, the portions covering the first 10 years of the graphs may be overlooked. The sequential MK analysis/graphs on the original annual flow and precipitation series were also used to examine and determine the possible starting time point (years) in which the apparent trends started to appear. The results obtained from the different stations can be compared in order to see whether the starting times shared any similarity.

### 4.6. Determining the most dominant periodic components for trends

The procedures for determining the periodic component(s) that are most dominant for trends in a time series consisted of two parts. Firstly, the sequential MK graphs of each detail components (with its approximation added) were examined with respect to their original data. These comparisons were done in order to find the detail components (with approximation added) whose progressive trend lines behave in the most similar manner with respect to their original data. Secondly, the MK *Z*-value for each of the detail components was compared to the MK *Z*-value of the original data to see if they are close (even if the values were not statistically significant). The periodic component(s) that satisfied these two requirements were considered the most dominant periodicities affecting the production of trends. In determining the most influential periodic component for trends, different combinations of detail components were also tried and tested. For example, if a time series was decomposed into four decomposition levels, we also tested several combinations of detail components (with the approximation added) such as D1 + D2 + A4, etc. We found that the results of using these combinations were not always conclusive. For example, the most dominant periodicity for station Richelieu River is the D4 component (with approximation) (Table 9; see Section 5.4) but in a combination of D3 + D4 (with approximation), the MK *Z*-value increased very significantly to +8.05. This is not close to the MK *Z*-value of the original data, and its sequential MK graph was not harmonious with the original data. Hence, we chose to only present the results using individual detail components (with its approximation added). This provides clearer information about the most dominant periodicities responsible for trends because of the closeness of the MK *Z*-values (between the individual most dominant periodic mode and the original data) and the sequential MK graph (which showed a harmonious trend line between the individual most dominant periodic mode and the original data). This was not always observed when the different detail components were combined.

## 5. Results and discussions

### 5.1. Preliminary data analysis

Flow and total precipitation time series (from the beginning of 1954 to the end of 2008) from eight flow stations and seven meteorological stations in Quebec and Ontario were analyzed for trends. First, the autocorrelation analysis was applied to each of the monthly, seasonally-based, and annual data flow and precipitation series in order to determine the significance of the lag-1 autocorrelation and to assess seasonality patterns. The summaries of flow and precipitation ACF values for their monthly, seasonally-based, and annual data are presented in Tables 3 and 4, respectively.

As can be seen, the serial correlation in the flow series is more pronounced compared to that of the precipitation series. This is perhaps due to the nature of Nordic rivers, which have flows that may lag by many months (Anctil and Coulibaly, 2004). The seasonality patterns were then visually determined based also on these correlograms. All monthly and seasonally-based data for both streamflow and precipitation show patterns of seasonality; the cycles are much clearer in flow data. The presence of strong annual cycles – especially in the flow data – is seen and indicated by the high ACF values that repeat at about every 12th lag (for monthly data) and every 4th lag (for seasonally-based data) – see Figs. 2 and 3 for examples. The influence of this yearly cycle on trends is looked into in more detail in the seasonally-based data analysis, where the second level of decomposition represents the 12-month periodic mode.

Three MK tests were employed to examine the presence of trends in the original time series and those resulting from the wavelet decomposition. Ideally, the modified MK test by Hirsch and Slack (1984) should be used when a time series shows a sea-

**Table 3**
Lag-1 Autocorrelation Functions (ACFs) of the original monthly, seasonally-based, and annual flow series.

| Flow station | Monthly data | Seasonally-based data | Annual data |
|---|---|---|---|
| Neebing River | 0.34* (S) | −0.20* (S) | 0.25 |
| North Magnetawan River | 0.27* (S) | −0.25* (S) | 0.08 |
| Black River | 0.42* (S) | −0.13* (S) | 0.09 |
| Sydenham River | 0.43* (S) | −0.07 (S) | 0.21 |
| Nagagami River | 0.41* (S) | −0.07 (S) | 0.05 |
| Missinaibi River | 0.32* (S) | −0.26* (S) | 0.13 |
| Eaton River | 0.19* (S) | −0.31* (S) | 0.07 |
| Richelieu River | 0.69* (S) | 0.10* (S) | 0.34* |

(S) Indicates the presence of seasonality cycles.
* Indicates significant lag-1 serial correlations at $\alpha = 5\%$.

**Table 4**
Lag-1 Autocorrelation Functions (ACFs) of the original monthly, seasonally-based, and annual precipitation series.

| Precipitation station | Monthly data | Seasonally-based data | Annual data |
|---|---|---|---|
| Fort Frances A | 0.30* (S) | −0.03 (S) | −0.02 |
| Sudbury A | 0.09* (S) | −0.02 (S) | 0.03 |
| North Bay A | 0.12* (S) | 0.02 (S) | 0.21 |
| Ottawa CDA | 0.02 (S) | −0.02 (S) | 0.19 |
| Windsor A | 0.06* (S) | 0.03 (S) | −0.22 |
| Montreal/Pierre Elliot Trudeau | 0.08* (S) | −0.04 (S) | 0.28* |
| Bagotville A | 0.02 (S) | 0.05 (S) | 0.06 |

(S) Indicates the presence of seasonality cycles.
* Indicates significant lag-1 serial correlations at $\alpha = 5\%$.

sonality pattern (with or without a significant autocorrelation). If a time series only exhibits a significant autocorrelation without the seasonality effect, the modified MK by Hamed and Rao (1998) should be used. The original MK test should be used when a time series exhibits neither a seasonality pattern nor significant lag-1 ACFs.

In order to examine how the trends have progressed over time, the sequential MK tests were applied to the original data and to the time series of the different periodic components obtained from the discrete wavelet decomposition. It is important to examine the sequential MK values because a mix of positive and negative trends may be present in the same time series. The sequential MK analysis can also help to determine how the trend of a detail component may explain the trends found in the original data. Indeed, in this study, the behavior of the trend lines of the detail components (plus approximation) is important. Therefore, not only the MK *Z*-values of these details are considered when determining the most influential periodic component(s) on the trend, but also how similarly their trend lines fluctuate with respect to trend line of the original data.

### 5.2. Monthly data analysis

Each monthly average flow and total precipitation dataset was decomposed into six lower resolution levels via the DWT approach. The detail components represent the 2-month periodicity (D1), 4-month periodicity (D2), 8-month periodicity (D3), 16-month periodicity (D4), 32-month periodicity (D5), and 64-month periodicity (D6). The A6 represents the approximation component at the sixth level of decomposition. Examples of the application of the discrete wavelet transform on monthly flow and precipitation series are shown in Figs. 4 and 5, respectively. These figures show the results when the DWT technique is used to decompose a time series. As can be seen, the lower detail levels have higher frequencies, which represent the rapidly changing component of the dataset, whereas the higher detail levels have lower frequencies, which represent the slowly changing component of the dataset. The approximation components (A6) in Figs. 4 and 5 represent the slowest changing component of the dataset (including the trend). It should be noted that due to space limitation, the results of every station are not presented graphically. The authors of this paper chose to only include the results of several stations, which were chosen with the purpose of illustrating the application of the DWT technique in conjunction with the MK trend test.

#### 5.2.1. Monthly average flow data

The application of the MK test on the eight original flow series over the study period showed a mix of positive and negative trends. Increasing trends are seen as being more dominant since five out of the eight flow stations show positive trend values. Three

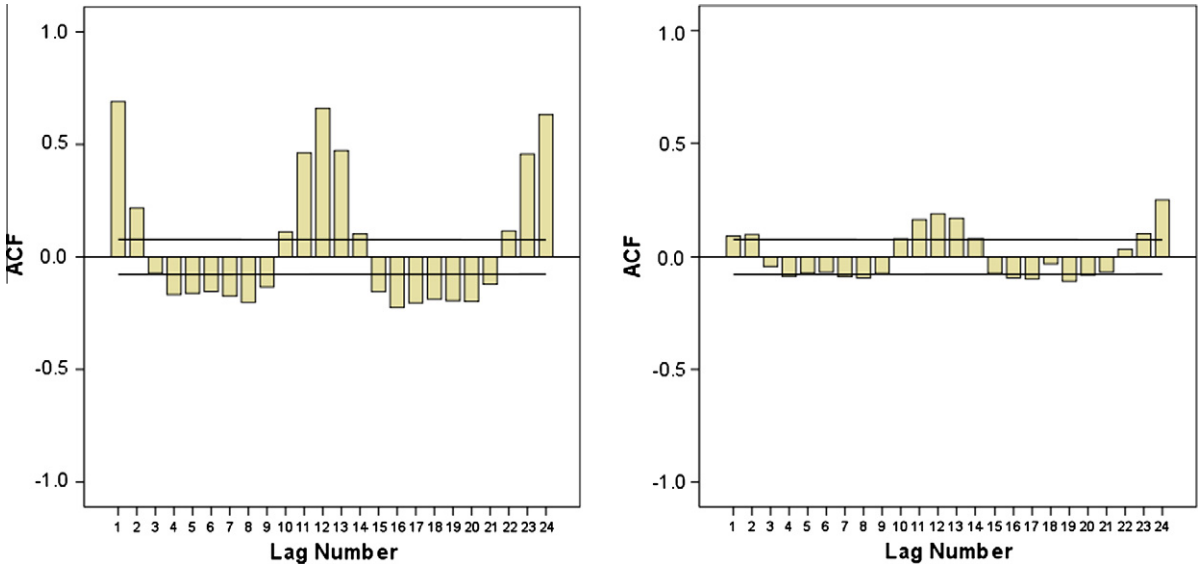


**Fig. 2.** Examples of annual cycles in the monthly series (left: Richelieu River; right: Montreal/Pierre Elliot Trudeau) are seen in these correlograms as there are higher ACF values at every 12th lag. The upper and lower solid lines represent the confidence intervals.

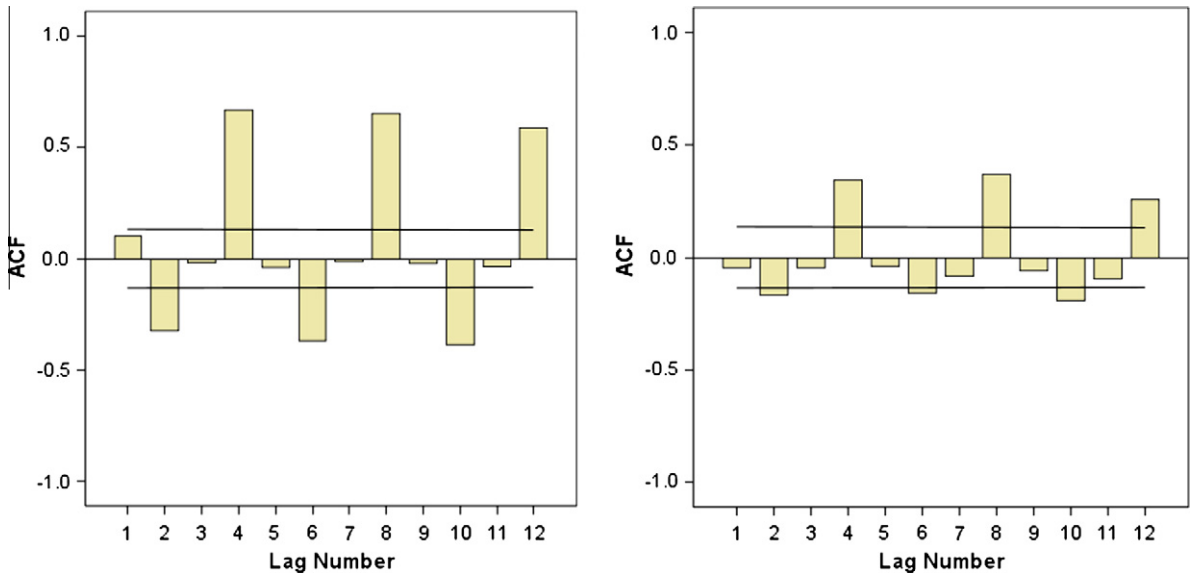


**Fig. 3.** Annual cycles are also seen in the seasonally-based series (left: Richelieu River; right: Montreal/Pierre Elliot Trudeau), where the values of ACFs at every 4th lag are higher compared to the other lags. The upper and lower solid lines represent the confidence intervals.

stations experience significant trend values, two being positive (Sydenham River and Richelieu River) and one negative (Missinaibi River). Table 5 shows the MK values for the original series, their detail components (Ds), approximations (A6), and the combination of the Ds with the approximation added to them. It can be seen in Table 5 that except for the D1 components of Black River ($Z = 2.00$) and Eaton River ($Z = 1.96$), none of the MK values of the different individual details (D1–D6) is statistically significant, even for stations whose original series showed significant MK values. For Sydenham River, Richelieu River, and Missinaibi River – whose original MK $Z$-values are significant, their approximation (A6) trend values are also significant.

A very interesting finding is that after the approximation components (A6) were added to the different details, many of the trend values became statistically significant. This is not only observed for stations with significant original trend values (i.e. Sydenham River, Missinaibi River, and Richelieu River), but also North Magnetawan River, which did not have a significant original trend value ($Z = +1.09$). This is perhaps due to MK $Z$-value of the A6 component being relatively high ($Z = 1.85$). Higher MK $Z$-values were also obtained in most cases, after the addition of the A6, compared to the MK values of the corresponding detail (D) alone (Table 5). In addition, the trend directions after the addition of A6 are also always in agreement with those of the corresponding original data (except for the D1 component for station Eaton River). It is clear that the approximation components have an effect on the original data because these approximations should carry most of the trend component. Furthermore, as supported by the information in Table 5, the results of the MK trend analysis on the detail components can be better interpreted after the addition of their respective approximation components. In light of these observations, graphs presented in this study are of the detail components with their respective approximations added. Discussions concerning the detail components also refer to the details plus their approximations. This is also applied to the seasonally-based and the annual data analysis, for both flow and precipitation variables.

Since all of the monthly flow data exhibit significant lag-1 ACFs and clearly portray seasonality patterns, the MK values presented in Table 5 were obtained by using the modified MK test by Hirsch and Slack (1984), which accounts for seasonality and autocorrelation factors. The detail components (with A6) that are considered to be the most representative of the trend in the original data are indicated in Table 5. The dominant periodic components vary from one station to another, which could be due to their different locations and sizes of drainage area. Generally speaking, the most influential periodicities over the study area are between D3 and D5. This indicates that the events between 8 and 32 months are the main drivers behind the observed trends. An example of how sequential MK graphs of the different periodic components portray their trend lines with respect to those of the original data is shown in Fig. 6 (station used: Sydenham River). As for the D1 components of the Black River and Eaton River stations, it is seen that they are not the best representative periodic mode and after the addition of the A6 components, the MK $Z$-values became insignificant. This suggests that the 2-month periodicity is not contributing to the trend for the Black River and Eaton River stations. It also makes sense that the D1 periodicity for these stations is not the most dominant mode, because even though their MK $Z$-values are significant, the trend values of the original data are not significant.

### 5.2.2. Monthly total precipitation data

For the monthly precipitation data, all the MK values for the original data were positive, except for station Montreal/Pierre Elliot Trudeau, which has a very weak negative trend value ($Z = -0.0049$). Three stations – North Bay A, Ottawa CDA, and Windsor A – had statistically significant upward trend directions with $Z = +3.67$, $+2.39$, and $+2.38$, respectively. After applying the MK test separately to the detail (D1–D6) and approximation (A6) components of each of the precipitation series, relatively similar findings were encountered to those of the flow results. None of the individual detail components alone showed significant MK values, even for the precipitation stations whose original series exhibited significant trends (Table 6). Only after the addition of the A6 component did several MK values become statistically significant.

Due to the presence of seasonality cycles, and in some, autocorrelation, the MK test by Hirsch and Slack (1984) was used in the monthly total precipitation data analysis. The results of the monthly precipitation data analysis show how the approximation components of the decomposition affect the detail components by increasing their trend values (in most cases) as reflected by the higher MK values (Table 6). This shows that the trend component is indeed contained within the approximation part of the wavelet transform,

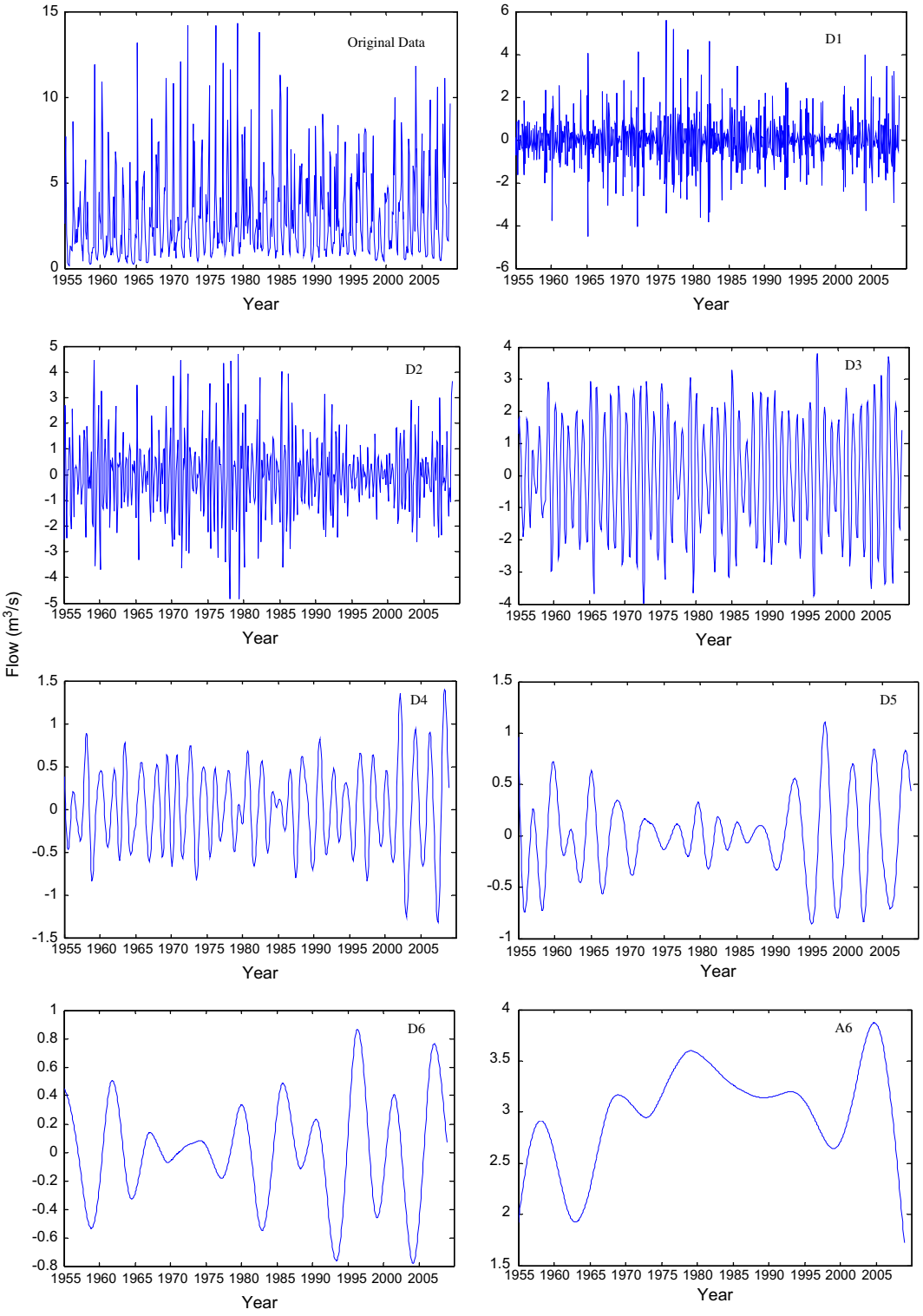


**Fig. 4.** Sydenham River's original monthly flow series and its transforms via the DWT using db9 wavelet, into six decomposition levels (D1–D6) and one approximation (A6).

implying that the trends are changing slowly and gradually (see the A6 graphs in Figs. 4 and 5); and are perhaps long-term. Some of the long-term trend values are statistically significant, as shown by the $Z$ values of the approximation components in Table 6. The abrupt fluctuations can be considered noise and are reflected in the lower details (Ds) – these alone are not significant. Table 6 also shows that for most of the stations higher periodic modes (especially D5) are more prominent in affecting the trend structures found in the monthly total precipitation data. As with the flow monthly data analysis, the trends are mostly affected by higher periodicities (low-frequency events). Here, the importance of decomposing a dataset prior to analyzing its trends using the wavelet transform is highlighted. Although the application of the MK test on the original data did not necessarily show the presence of significant trends, the

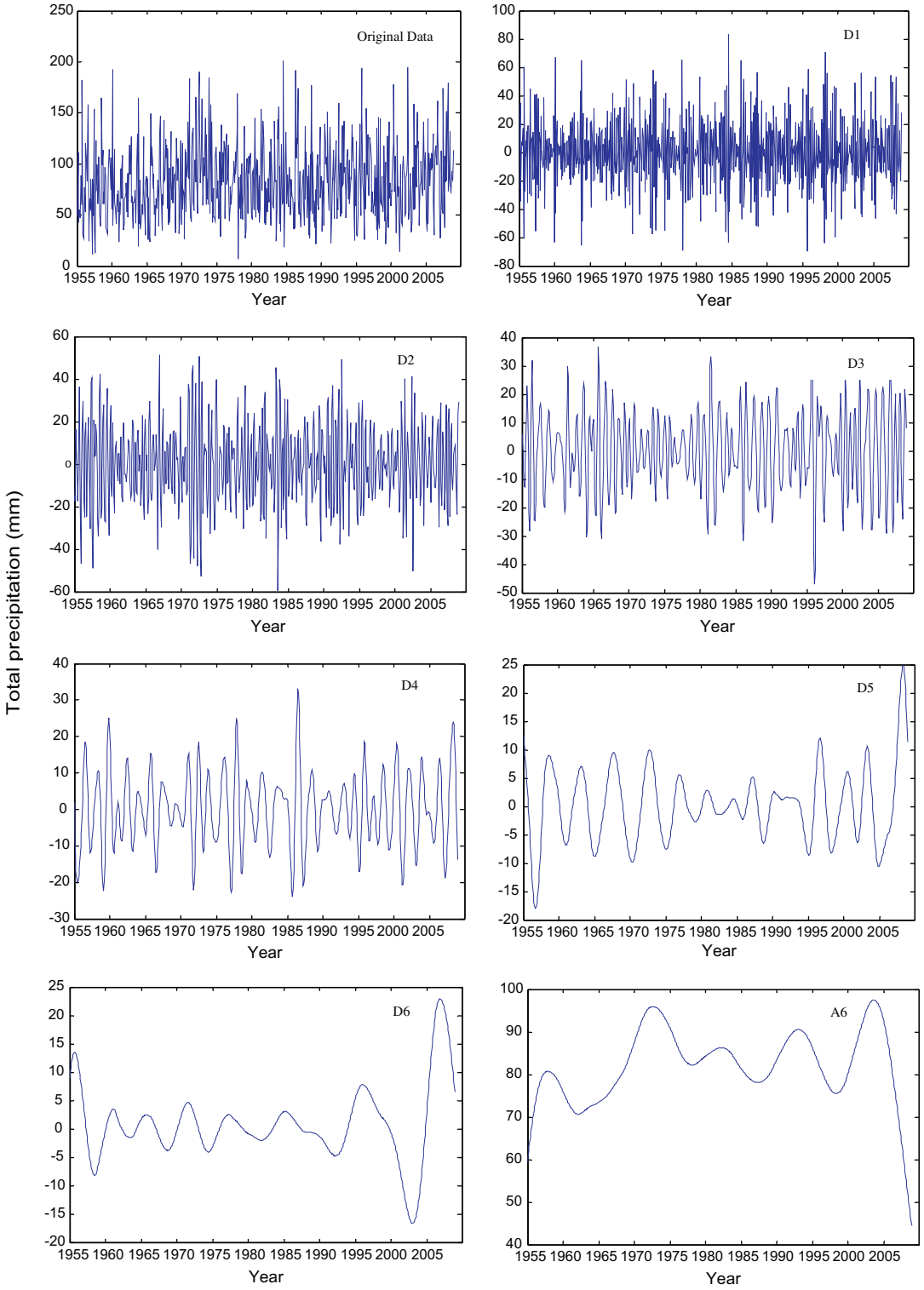


**Fig. 5.** Montreal/Pierre Elliot Trudeau's original monthly flow series and its transforms via the DWT using db9 wavelet, into six decomposition levels (D6–D6) and one approximation (A6).

results of the application of the MK test on the decomposed data may reveal some significant values.

### 5.3. Seasonally-based data analysis

The presence of annual cycles in the monthly-based time series analysis led us to incorporate the seasonally-based data in our trend analysis. Again, the seasonally-based data also confirms the presence of annual cycles in some datasets as the ACFs show high values at every 4th lag (examples are given in Fig. 3). Each seasonally-based time series was decomposed into four detail components (D1–D4) and one approximation (A4). D1, D2, D3, and D4 represent the 6-month, 12-month, 24-month, and 48-month fluctuations, respectively. The A4 component corresponds to the

**Table 5**
Mann–Kendall values of the monthly flow series: original data, details components (D1–D6), approximations (A6), and a set of combination of the details and their respective approximations. The most effective periodic components for trends are indicated in bold format.

| Data | Neebing River | N. Magnetawan River | Black River | Sydenham River | Nagagami River | Missinaibi River | Eaton River | Richelieu River |
|---|---|---|---|---|---|---|---|---|
| Original | −0.26 | 1.09 | 1.26 | 3.10* | 1.19 | −2.05* | −0.42 | 3.18* |
| D1 | −0.64 | 0.68 | 2.00* | −0.95 | 0.52 | −1.25 | 1.96* | −0.39 |
| D2 | −0.37 | −0.20 | 0.38 | −0.46 | −1.09 | 0.85 | −0.12 | −0.38 |
| D3 | 0.50 | 0.22 | 0.77 | 0.87 | −0.32 | −0.10 | 0.00 | 0.73 |
| D4 | 0.00 | −0.36 | −0.10 | 0.06 | 0.06 | −0.28 | −0.21 | 0.12 |
| D5 | −0.06 | −0.28 | −0.20 | −0.02 | 0.06 | −0.06 | 0.03 | −0.18 |
| D6 | −0.18 | −0.30 | 0.23 | 0.15 | 0.22 | 0.01 | 0.50 | 0.35 |
| A6 | −1.17 | 1.85 | 1.17 | 3.08* | 1.20 | −3.69* | −0.38 | 3.37* |
| D1 + A6 | −1.01 | 2.47* | 1.56 | 3.47* | 1.26 | −3.05* | 0.14 | 3.54* |
| D2 + A6 | −0.81 | 2.50* | 1.44 | 3.66* | 0.51 | **−2.53*** | −0.15 | 3.66* |
| D3 + A6 | −1.00 | 2.60* | 1.11 | **3.07*** | 1.05 | −2.73* | −0.10 | 3.44* |
| D4 + A6 | **−0.92** | 2.34* | **1.17** | **2.95*** | **1.22** | −2.70* | −0.49 | 3.23* |
| D5 + A6 | **−0.76** | **1.90** | 1.13 | **2.61*** | **1.17** | **−2.68*** | **−0.37** | **2.91*** |
| D6 + A6 | −1.62 | 2.25* | 0.99 | 3.69* | 1.15 | −2.94* | **−0.38** | 3.64* |

* Indicates significant trend values at $\alpha = 5\%$.

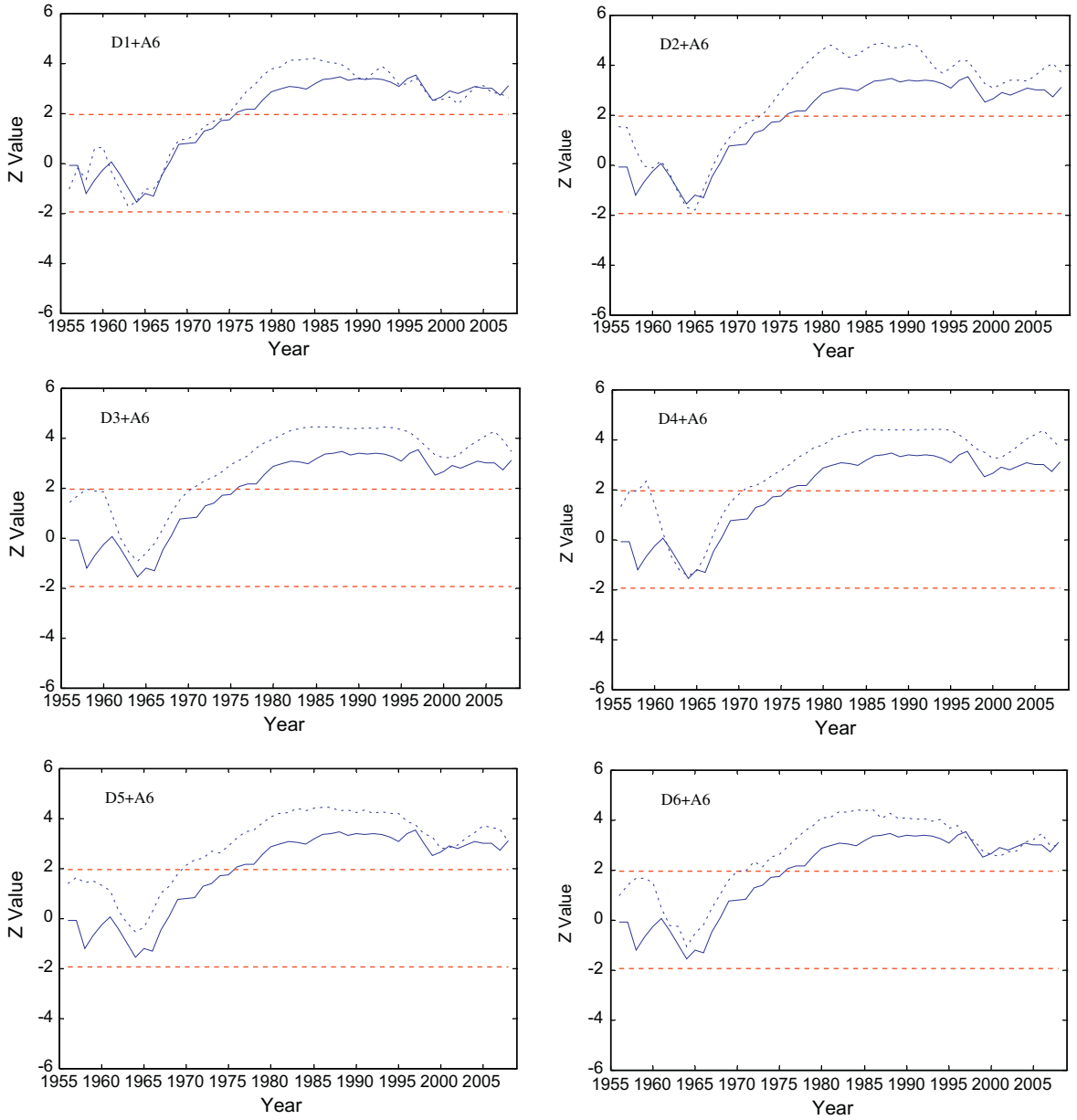


**Fig. 6.** Sequential Mann–Kendall graphs of station Sydenham River monthly data displaying the progressive trend lines of each detail (with the approximation added). The upper and lower dashed lines represent the confidence limits ($\alpha = 5\%$); the solid and dashed progressive lines are the original and detail sequential MK lines, respectively.

approximation of the fourth decomposition level. As can be seen, the D2 component in the seasonally-based data decomposition represents the annual (12-month) periodicity. This is very useful in determining whether or not the annual cycles can explain the trends found in the flow and precipitation data.

Most of the first level of decomposition (D1) of the seasonally-based series – and sometimes the D2 component as well – portray a strong yearly cycle because the corresponding ACF values are high at every 4th lag (illustrated in Fig. 7). The repeating cycles do not dampen over time. Oscillating patterns may also be observed at higher decomposition levels, but they dampen as the number of lags increases (see Fig. 8 for example). Similar behavior was also seen in the components resulting from the addition of each detail to its approximation (D + A4). The oscillations observed in the correlograms of the lower decomposition levels are actually expected because they should capture the oscillating properties (such as the seasonality) of the time series, thus filtering the stochastic components of the time series (Popoola, 2007). On the other hand, the ACFs of the approximation component should not have any oscillating behavior or behave in the manner of seasonal fluctuations, even if the original time series shows seasonality patterns (Popoola, 2007). Fig. 9 displays the ACFs of several approximation components (A4 in this case); as can be seen, there is an absence of oscillatory patterns.

*5.3.1. Seasonally-based average flow data*

As with the monthly flow data analysis, there is also a mix of positive and negative trends observed in the seasonally-based flow data. In fact, the directions of trend of the seasonally-based datasets are in agreement with the directions of their monthly data counterparts. For example, Neebing River, Missinaibi River and Eaton River stations experience negative trends in their monthly data, and also in their seasonally-based data. Only two out of the eight flow stations showed statistically significant trends: Sydenham River ($Z = +3.13$) and Richelieu River ($Z = +3.06$) (Table 7).

Table 7 shows that none of the individual detail components alone (including D2) showed statistically significant MK $Z$-values. Again, after the addition of the A4s to their respective details, many of the MK $Z$-values became higher and statistically significant, emphasizing that the approximations carry most of the trend component. An example of the sequential MK analysis is shown in Fig. 10 (station used: Sydenham River).

**Table 6**
Mann–Kendall values of the monthly precipitation series: original data, details components (D1–D6), approximations (A6), and a set of combination of the details and their respective approximation. The most effective periodic components for trend are indicated in bold format.

| Data | Fort Frances A | Sudbury A | North Bay A | Ottawa CDA | Windsor A | Montreal/Pierre Elliot Trudeau | Bagotville A |
|---|---|---|---|---|---|---|---|
| Original | 0.71 | 1.85 | 3.67* | 2.39* | 2.38* | −0.0049 | 0.75 |
| D1 | −0.23 | −0.68 | −0.83 | −1.09 | 0.01 | 0.01 | −0.10 |
| D2 | 0.34 | −0.68 | 0.18 | −0.03 | −0.05 | 0.65 | 0.39 |
| D3 | −0.70 | −0.32 | −0.60 | 0.23 | −0.30 | −0.27 | −0.93 |
| D4 | 0.18 | −0.13 | −0.03 | 0.15 | −0.04 | −0.16 | 0.34 |
| D5 | 0.02 | 0.27 | 0.14 | −0.17 | 0.50 | 0.28 | 0.02 |
| D6 | −0.33 | 0.12 | 0.15 | 0.16 | 1.00 | 0.53 | 0.43 |
| A6 | 0.63 | 2.04* | 4.18* | 2.41* | 3.47* | 0.08 | 0.77 |
| D1 + A6 | 1.20 | 2.59* | 3.43* | 1.98* | 2.87* | 0.07 | 1.58 |
| D2 + A6 | 1.79 | 2.72* | 3.85* | 2.01* | 3.05* | 0.73 | 1.03 |
| D3 + A6 | 1.28 | 2.62* | 3.78* | 2.12* | 3.43* | −0.23 | 0.92 |
| D4 + A6 | 1.01 | 2.06* | 3.45* | 1.85 | 1.87 | **−0.08** | 1.08 |
| D5 + A6 | **0.76** | **1.79** | **3.64*** | 2.00* | **2.84*** | **0.22** | **0.73** |
| D6 + A6 | 1.03 | 2.98* | 4.15* | **2.68*** | 2.93* | 0.61 | 1.29 |

* Indicates significant trend values at $\alpha = 5\%$.

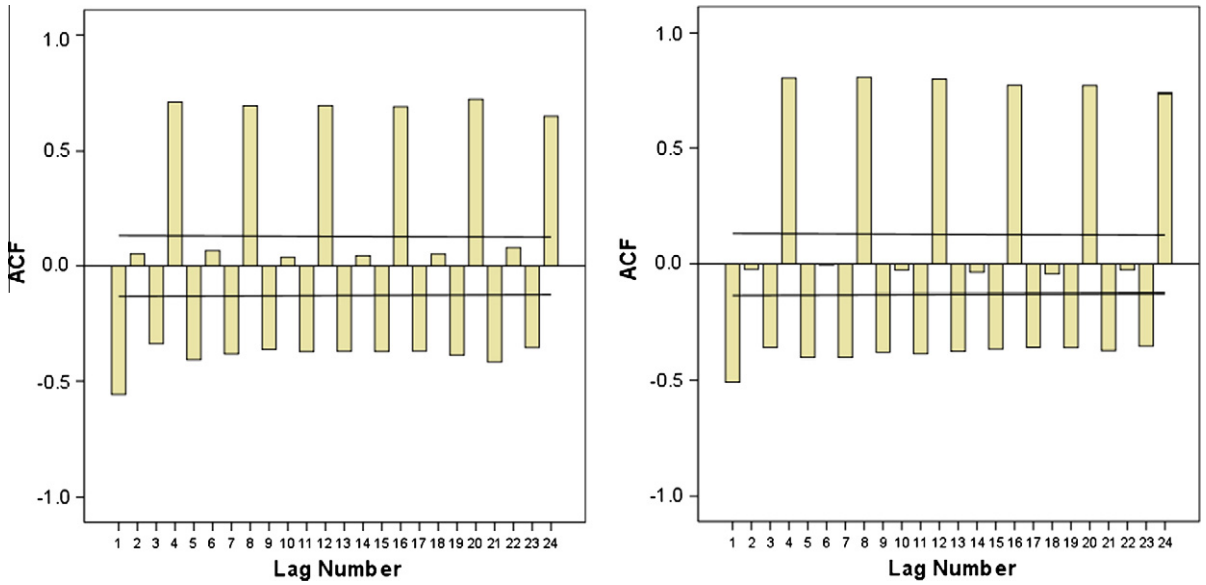


**Fig. 7.** Examples of correlograms of the D1 periodic components (left: Neebing River; right: Missinaibi River) of the seasonally-based data, which display strong annual cycles as seen in their repeated high values at every 4th lag. Note that the cycles do not dampen over time.

As shown in Table 7, none of the most dominant periodicities were represented by the D1 component, indicating that the 6-month fluctuation is not responsible for the observed trend. There are four stations for which the D2 components represent one of the most dominant periodicities affecting the observed trends. These stations are: Black River, Nagagami River, Missinaibi River, and Eaton River. Therefore, for these stations, their trends are affected by the annual periodicities (the MK sequential graphs for these D2 components are given in Fig. 11). The D3 and D4 components, which represent the 24- and 48-month time modes, are also seen to be important in affecting the trends.

It can be seen that the seasonally-based data are important variables to be included to assess the flow and precipitation trends in this study. This is because the monthly-based data analysis skipped the 12-month time scale as the third and fourth dyadic scales in the monthly data decomposition correspond to 8 and 16 months, respectively.

*5.3.2. Seasonally-based total precipitation data*

All the MK *Z*-values for the original seasonally-based total precipitation data showed positive trends (Table 8); three stations experienced statistically significant trends: North Bay A ($Z = 2.81$), Ottawa CDA ($Z = 2.31$), and Windsor A ($Z = 2.39$), which is in agreement with the results of the monthly total precipitation data. Again, it is seen that none of the individual detail components show significant trend values. Significant trends that were observed for A4 components belong to the three stations that have significant original trend values. The MK values of the detail components for the stations whose A4 components were not significant (Fort Frances, Sudbury A, Montreal/Pierre Elliot Trudeau, and Bagotville A) remain insignificant even after the addition of their respective approximations. This may indicate that the long-term trends for these stations are not statistically significant as shown by their A4 components of the annual data, which were indeed insignificant and have the lowest absolute MK *Z*-values (see the following subsections).

Table 8 also shows the periodic components that are the most influential in affecting the trends in the seasonally-based total precipitation data. It is seen that the annual periodicity (D2) does not contribute to the trend production in the total precipitation data. This insignificant contribution can also be partly explained by the weaker annual cycles observed in the precipitation data, in

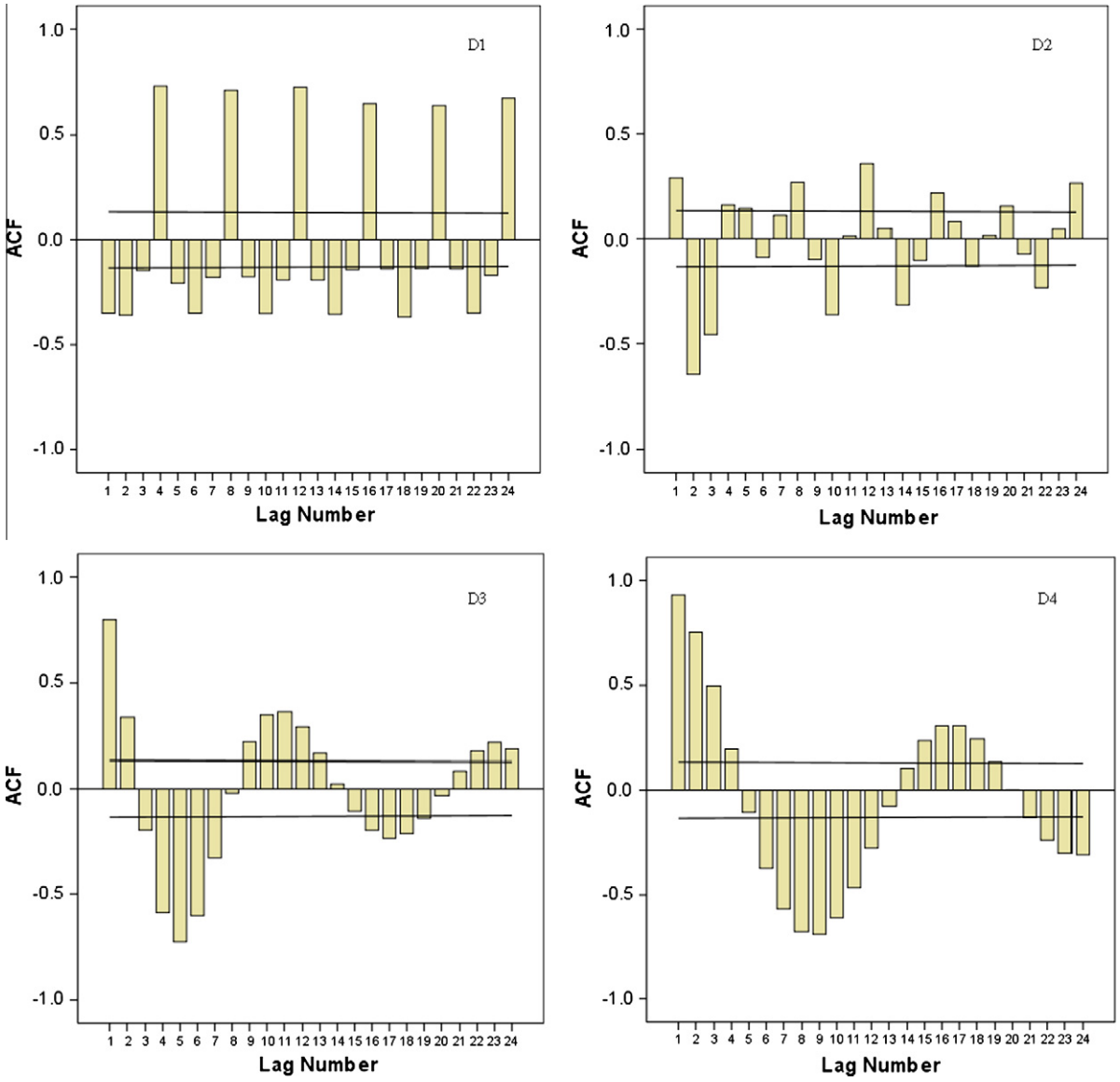


**Fig. 8.** The correlograms of the D1–D4 components of Nagagami River's seasonally-based data. The D1 and D2 components have high ACF values at every 4th lag, which indicates the presence of 12-month cycles. D3 and D4 show some patterns of oscillations that may dampen over time, which are not considered annual cycles.

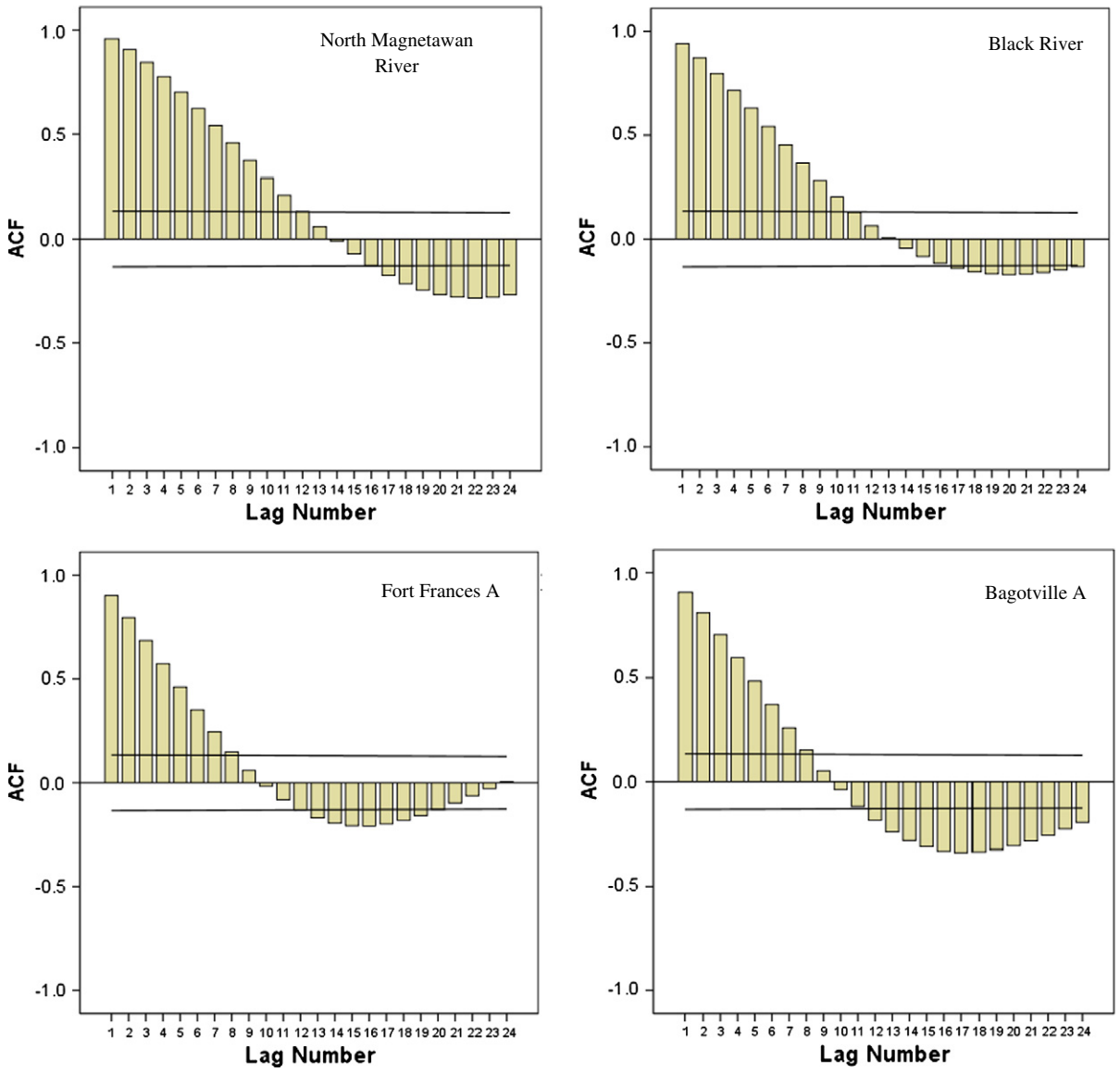


**Fig. 9.** The correlograms of several approximation components (A4) of the seasonally-based data showing a lack of constant oscillations.

**Table 7**
Mann–Kendall values of the seasonally-based flow series: original data, details components (D1–D4), approximations (A4), and a set of combination of the details and their respective approximations. The most dominant periodic components for trend are indicated in bold format.

| Data | Neebing River | N. Magnetawan River | Black River | Sydenham River | Nagagami River | Missinaibi River | Eaton River | Richelieu River |
|---|---|---|---|---|---|---|---|---|
| Original | −0.27 | 1.43 | 1.36 | 3.13* | 1.31 | −1.78 | −0.22 | 3.06* |
| D1 | −0.43 | −0.20 | 0.89 | −0.85 | 0.60 | −0.43 | −0.06 | −0.45 |
| D2 | −0.05 | 0.44 | −0.46 | 0.61 | −0.07 | 0.14 | 0.01 | 0.00 |
| D3 | 0.21 | −0.59 | 0.16 | −0.29 | 0.01 | 0.18 | 0.05 | 0.05 |
| D4 | 0.10 | 0.52 | 0.38 | −0.27 | 0.00 | 0.14 | −0.11 | −0.04 |
| A4 | −1.10 | 1.43 | 1.24 | 2.99* | 1.53 | −3.59* | −0.77 | 3.52* |
| D1 + A4 | −0.82 | 2.36* | 0.91 | 3.75* | 1.76 | −3.19* | −0.72 | 3.70* |
| D2 + A4 | −0.99 | 2.09* | **1.52** | 3.73* | **1.14** | **−2.32*** | **−0.53** | 3.76* |
| D3 + A4 | **−0.45** | **1.64** | 0.92 | 2.54* | 1.80 | **−2.48*** | **−0.54** | **2.97*** |
| D4 + A4 | −1.05 | **1.83** | **0.81** | **3.47*** | **1.36** | −2.81* | −1.17 | **3.51*** |

* Indicates significant trend values at $\alpha = 5\%$.

comparison to the flow data. Most of the precipitation trends are affected by the D3 and D4 components, except for station North Bay A, where D1 is considered the most dominant periodic component. We can suggest that the periodic components that mainly affect trends in the seasonally-based total precipitation are the 24- to 48-month time scales (2–4 years). An example of the sequential MK graphs for the different periodic components portraying their trend lines with respect to their original data is given in Fig. 12 (station used: Ottawa CDA).

### 5.4. Annual data analysis

The trend analysis of the monthly and seasonally-based data suggests that there is a possibility of longer time-periodicity than

just 48 and 64 months (which are the last periodic modes in the seasonally-based and monthly data decompositions, respectively). Many of the trends in the monthly and seasonally-based data are influenced by the higher time periodic components (i.e. lower-frequency events). The argument that there may be higher time periodicities affecting the trend in streamflow and precipitation is also reflected in the approximation components of the DWTs, which should carry the trend element (slowest-changing events) of the time series: (1) many approximation components in the data analysis showed significant MK $Z$-values; and (2) higher MK $Z$-values of the detail components were observed after the addition of their respective approximations. Annual time series were then analyzed in order to obtain a more thorough trend analysis. Each annual time series was decomposed into four levels, which correspond to the 2-year, 4-year, 8-year and 16-year variations.

Although there is a mixture of positive and negative trends in the annual flow, most of the stations exhibit positive trends. Three streamflow stations have experienced significant trend: Sydenham River ($Z = 2.37$), Missinaibi River ($Z = -2.23$), and Richelieu River ($Z = 2.92$) (Table 9). Indeed, most studies focusing on streamflow trends in Canada have generally found that the flow trends in Canadian rivers are not uniform. There are areas that experience positive trends while others are experiencing negative trends (due to factors such as temperature, amount of precipitation, and evapotranspiration).

For the annual total precipitation, only stations North Bay A ($Z = +3.57$) and Ottawa CDA ($Z = +2.50$) experienced significant trend values (Table 10). It is worth mentioning that all of the original annual precipitation data (as well as most of the monthly and seasonally-based precipitation data) show positive trend values – this prevalent increase in trends in the total precipitation seen in this study are in agreement with findings from several other precipitation studies. For example: Mekis and Hogg (1999) found that total annual precipitation in many parts of Canada is on the rise; Stone et al. (2000) reported that total annual precipitation in the south of Canada experienced an increase (from 1895 to 1996); Zhang et al. (2000) found that the total annual precipitation has increased across Canada by 5%-35%. Groleau et al. (2007) also found that 30% of the weather stations in southern Quebec and New Brunswick, Canada, experienced significant positive trends during winter rainfall.

The periodic component(s) considered the most influential in affecting trends in flow and precipitation data are indicated in Tables 9 and 10, respectively. Examples of determining the most dominant periodic components that affect the production of trends in annual flow and precipitation series are given in Figs. 13 and 14, respectively. There are a few individual detail components (without approximation) that showed significant trend values (Tables 9 and 10). However, these components do not end up being considered the most influential time periodicities to affect the trends. For example, in Table 9, the MK $Z$-value of the D4 component of Black River station is 2.38, but it is not found to be the most dominant periodic component for trend. It is also seen that the difference in MK $Z$-value between the D4 (with approximation) and the original data is high. It is therefore not expected that the D4 detail component in Black River station would be the most influential component to affect the trend. This illustrates that when analyzing trends in a dataset via the wavelet transform, not only should the final MK value for the different components be considered, but also their sequential MK values in comparison to the original data.

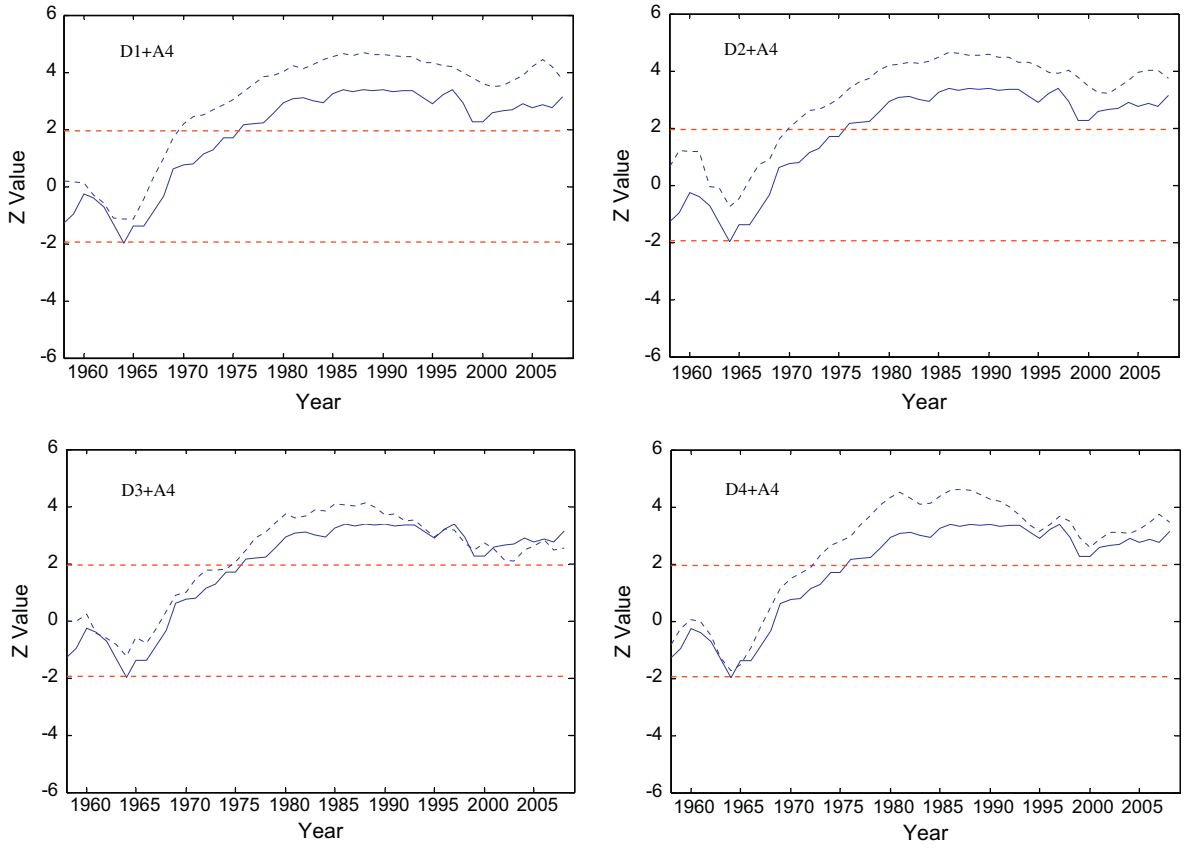


**Fig. 10.** Illustration of the sequential Mann–Kendall graphs of the D1–D4 components (with approximation) of the seasonally-based data in order to determine the most dominant periodic component for trend (Sydenham River's data were used in this example). The upper and lower dashed lines represent the confidence limits ($\alpha = 5\%$); the solid and dashed progressive lines are the original and detail component sequential MK lines, respectively.

Tables 9 and 10 show that the dominant periodic components playing major roles in affecting the trends in the annual data are not uniform. The most common dominant periodicities are D1 and D2 (both with approximations added). This is an indication that the trends in the annual data over the study area are mainly characterized by 2- to 4-year periodic events (inter-annual fluctuations).

The progressive MK graphs of the annual data give indications that most of the trends – positive or negative – visibly started during the period from 1965 to early 1970s (Figs. 15 and 16). This timing is important as it has been noticed in several Canadian studies that 1970 serves as a point of change in streamflow and precipitation activities in relation to the atmospheric variability affecting Canadian climate, such as the Pacific/North America teleconnection (PNA) and the North Atlantic Oscillation (NAO). Indeed, these periodic modes may also be associated with the North Atlantic Oscillation (NAO), which has one of its main peaks centered at 2 years (Cook et al., 1998; Anctil and Coulibaly, 2004). Fu et al. (2012), who studied the influence of solar activities and El Niño on streamflow in southern Canada, indicated that there is a correlation between streamflow activities and solar activities at 11 and 22 years. The correlation between streamflow activities in southern Canada and the El Niño cycles is at the 2–7 year periodicities (Fu et al., 2012). The combined effect of solar activities and El

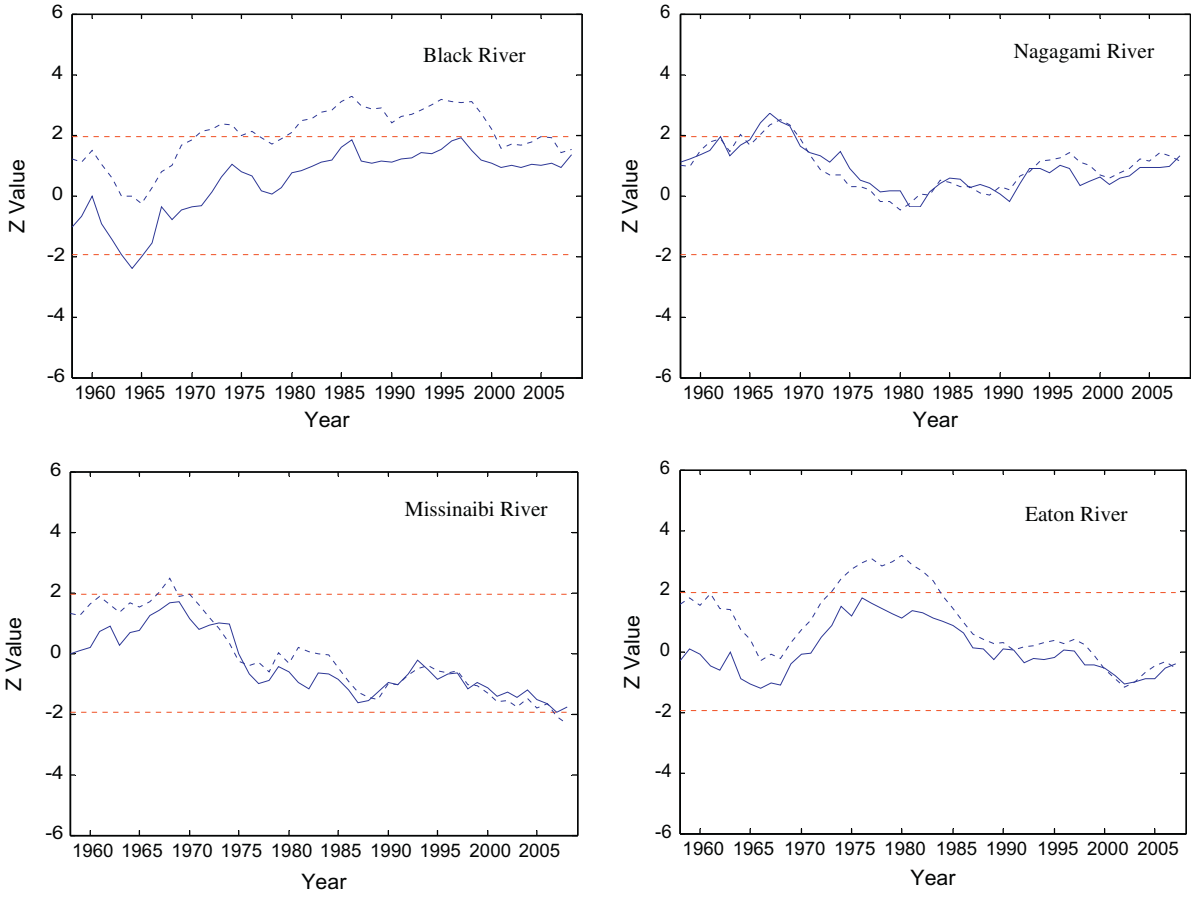


**Fig. 11.** Sequential Mann–Kendall graphs of the D2 components, which represent the 12-month periodic components from several seasonally-based flow data. These trend lines show good matches with respect their original trend lines. The upper and lower dashed lines represent the confidence limits ($\alpha = 5\%$); the solid and dashed progressive lines are the original and detail component sequential MK lines, respectively.

**Table 8**
Mann–Kendall values of the seasonally-based precipitation series: original data, details components (D1–D4), approximations (A4), and a set of combination of the details and their respective approximation. The most dominant periodic components for trends are indicated in bold format.

| Data | Fort Frances A | Sudbury A | North Bay A | Ottawa CDA | Windsor A | Montreal/Pierre Elliot Trudeau | Bagotville A |
|---|---|---|---|---|---|---|---|
| Original | 0.72 | 1.32 | 2.81* | 2.31* | 2.39* | 0.15 | 0.77 |
| D1 | 0.29 | −0.66 | −0.51 | 0.47 | −0.11 | −1.70 | −0.96 |
| D2 | 0.00 | 0.04 | −0.23 | −0.45 | 0.31 | 0.43 | 0.22 |
| D3 | 0.15 | 0.16 | −0.02 | 0.41 | −0.41 | −0.25 | 0.06 |
| D4 | 0.59 | 0.00 | 0.93 | 0.22 | −0.20 | −0.19 | 0.21 |
| A4 | 0.81 | 1.76 | 5.09* | 2.31* | 2.41* | 0.19 | 0.62 |
| D1 + A4 | 1.45 | 1.55 | **3.39*** | 2.94* | 2.09* | −0.17 | 0.64 |
| D2 + A4 | 0.21 | 1.53 | 4.13* | 2.17* | 2.23* | 0.03 | 0.63 |
| D3 + A4 | **0.64** | 1.55 | 4.01* | **2.35*** | 1.21 | −0.40 | 0.33 |
| D4 + A4 | 1.12 | **1.17** | 4.12* | **2.59*** | **2.36*** | **0.02** | **0.72** |

* Indicates significant trend values at $\alpha = 5\%$.

**Table 9**
Mann–Kendall values of the annual flow series: original data, details components (D1–D4), approximations (A4), and a set of combination of the details and their respective approximation. The most influential periodic components for trends are indicated in bold format.

| Data | Neebing River | N. Magnetawan River | Black River | Sydenham River | Nagagami River | Missinaibi River | Eaton River | Richelieu River |
|---|---|---|---|---|---|---|---|---|
| Original | −0.50 | 0.91 | 0.73 | 2.37* | 1.12 | −2.23* | −0.46 | 2.92* |
| D1 | −0.13 | 0.00 | −0.19 | −0.01 | 0.15 | −0.16 | 0.22 | 0.19 |
| D2 | −0.04 | 0.30 | 0.10 | −0.15 | 0.17 | −0.15 | 0.27 | 0.12 |
| D3 | 0.57 | −0.13 | 0.06 | 0.51 | 0.25 | −0.30 | −0.28 | 0.46 |
| D4 | −1.63 | 3.66* | 2.38* | 2.15* | 1.22 | −0.41 | −0.55 | 0.15 |
| A4 | −0.48 | 1.80 | 1.15 | 2.66* | 1.96* | −2.12* | −0.79 | 3.09* |
| D1 + A4 | **−0.57** | **1.39** | 0.55 | 1.42 | 0.49 | −1.73 | **−0.60** | 2.61* |
| D2 + A4 | **−0.73** | 1.55 | **0.68** | 1.47 | **0.96** | **−2.12*** | −0.87 | 2.98* |
| D3 + A4 | −0.19 | **0.94** | 0.80 | **2.51*** | 0.94 | −2.47* | −0.97 | 1.99* |
| D4 + A4 | −3.03* | 3.95* | 4.33* | 3.17* | 3.44* | −4.57* | −1.16 | **3.09*** |

* Indicates significant trend values at $\alpha = 5\%$.

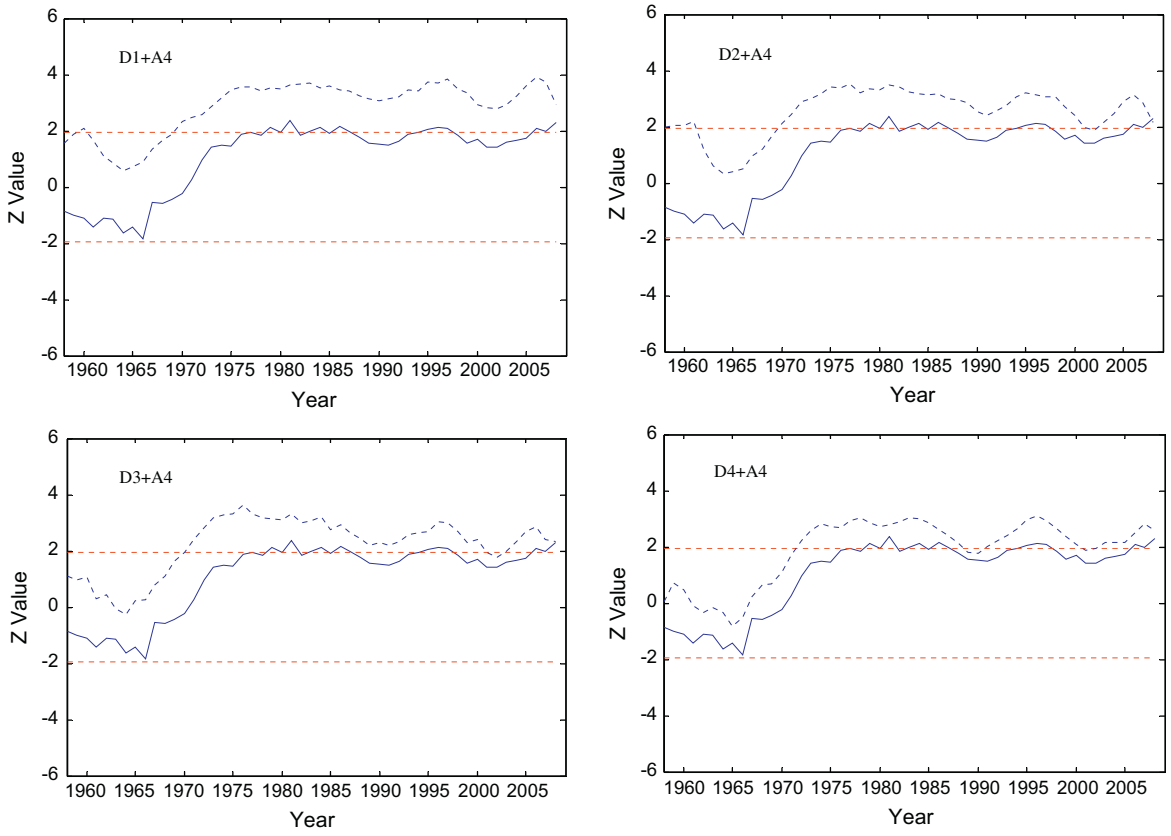


**Fig. 12.** Sequential Mann–Kendall graphs of the components of the seasonally-based precipitation data from Ottawa CDA station. The upper and lower dashed lines represent the confidence limits ($\alpha = 5\%$); the solid and dashed progressive lines are the original and detail sequential MK lines, respectively. Based on the MK values and the sequential MK graphs, D3 and D4 (with approximations) were determined to be the most effective periodic components contributing to the trend production.

**Table 10**
Mann–Kendall values of the annual precipitation series: original data, details components (D1–D4), approximations (A4), and a set of combination of the details and their respective approximation. The most influential periodic components for trends are indicated in bold format.

| Data | Fort Frances A | Sudbury A | North Bay A | Ottawa CDA | Windsor A | Montreal/Pierre Elliot Trudeau | Bagotville A |
|---|---|---|---|---|---|---|---|
| Original | 0.68 | 1.24 | 3.57* | 2.50* | 1.70 | 0.33 | 0.95 |
| D1 | 0.54 | −0.16 | −0.13 | −0.41 | 0.04 | 0.06 | −0.33 |
| D2 | 0.12 | −0.28 | 0.39 | 0.19 | 0.33 | 0.25 | −0.55 |
| D3 | 0.00 | −0.18 | 0.70 | 0.49 | 0.96 | 0.58 | 0.99 |
| D4 | 1.32 | 2.51* | 1.87 | 3.21* | 2.31* | −0.70 | 1.09 |
| A4 | 1.22 | 1.45 | 4.91* | 2.45* | 2.15* | −0.02 | 1.28 |
| D1 + A4 | **0.68** | **1.34** | 2.35* | 0.00 | **1.05** | **−0.31** | −0.29 |
| D2 + A4 | 1.06 | **1.39** | **3.51*** | 0.51 | **1.93** | **0.00** | −0.12 |
| D3 + A4 | 0.65 | 2.45* | 4.27* | **1.84** | 3.27* | 0.25 | **0.90** |
| D4 + A4 | 2.89* | 3.82* | 5.31* | 3.14* | 5.26* | −0.91 | 1.63 |

* Indicates significant trend values at $\alpha = 5\%$.

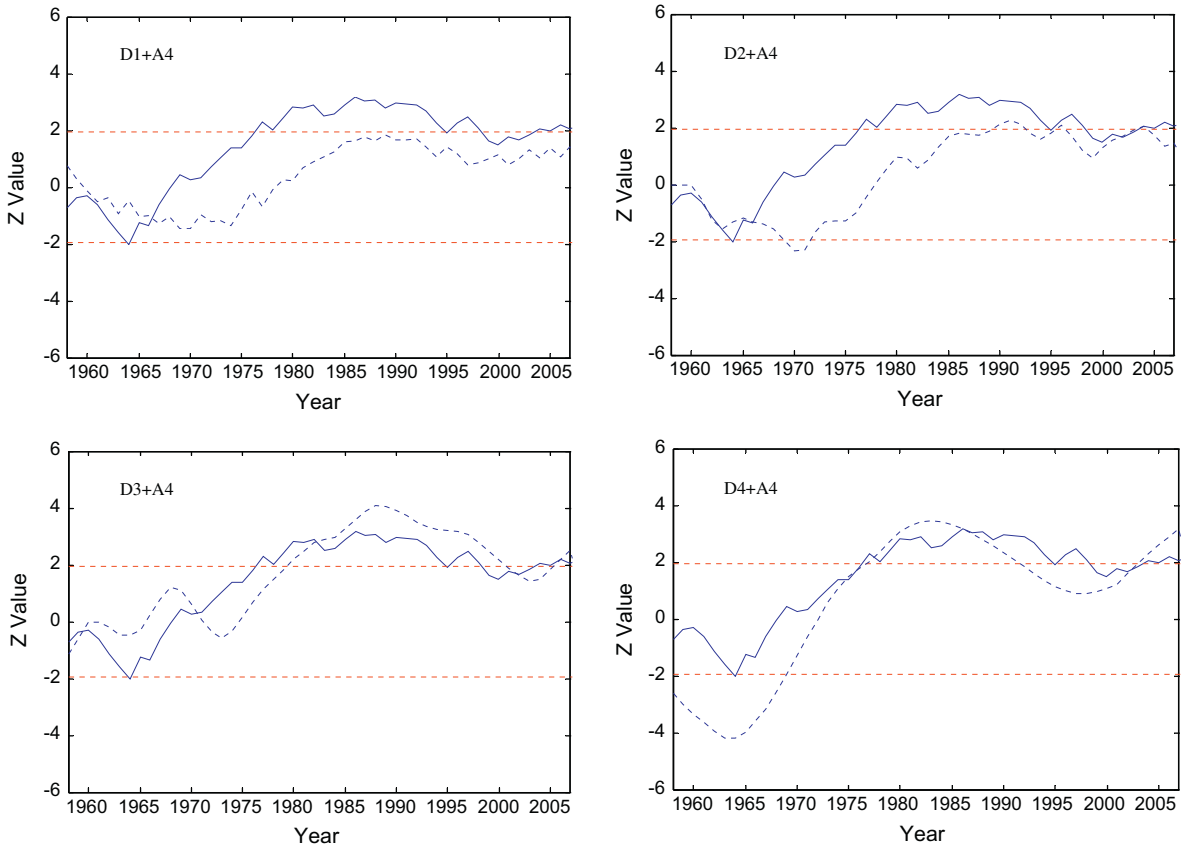


**Fig. 13.** Examples of sequential Mann–Kendall graphs of the detail components of the annual flow data in order to determine the most dominant periodicity for trends (Sydenham River's data were used in this example). The upper and lower dashed lines represent the confidence limits ($\alpha$ = 5%); the solid and dashed progressive lines are the original and detail sequential MK lines, respectively.

Niño is found at 18–32 years (Fu et al., 2012). Here, as can be observed in Table 9, the most common dominant periodicities are 2–4 years, which could also be related to the El Niño effect. The Richelieu River's most dominant periodicity is the 16-year mode, which may be a result of the combined effect of solar activities and the El Niño cycle. Prokoph et al. (2012) also found that the maximum annual streamflow activities in southern Canada have strong 11-year cycles, which match the 11-year solar radiation activities. It is also suggested that the effects of ENSO and NAO on precipitation, which in turn affect the streamflow activities in southern Canada, are also evident (Prokoph et al., 2012). It is very likely that multiple factors are affecting the precipitation and streamflow trends over the study area.

In Fig. 15 it is observed that at six out of the eight flow stations, there were upward trends that started between 1965 and 1970. In four out of these six stations, the trends stopped between 1980 and 1985, followed by either downward trends or no trends. Fig. 16 shows that positive trends started around 1965 at five out of the seven meteorological stations. Anctil and Coulibaly (2004), who analyzed the inter-annual variability of Quebec streamflow, also placed an importance on the year 1970 because there was a positive correlation between the streamflow activity (especially at the 2–3 year band) and the PNA index since around 1970. Similarly, Coulibaly and Burn (2004), who analyzed annual Canadian streamflow, also found 1970 as the change point in flow activity. They found that the PNA and the NAO are the main dominant teleconnection patterns for the period of 1950–1999 and after 1970, respectively (Coulibaly and Burn, 2004). Stone et al. (2000) studied the variability in Canadian precipitation and its intensity and related them to the PNA and NAO. Different seasons and regions responded differently to the atmospheric variation, but both the NAO and the PNA were found to have a statistical significance in affecting precipitation intensity over Canada. For example, the NAO (positive phase) has a significant impact, which affected the precipitation intensity during a few 3-month seasons in eastern Canada (Stone et al., 2000). The NAO has been in a positive phase since around 1970 (Anctil and Coulibaly, 2004). The PNA also significantly affected the precipitation increase during autumn and winter seasons in Ontario and southern Quebec, during the second half of the 20th century (Stone et al., 2000). Therefore, the trends observed in this study, both in flow and precipitation data, could be related to the activity of these influential hydro-climatic indices.

## 6. Conclusions and recommendations

The DWT and the MK tests were applied on the mean flow and total precipitation datasets, over southern parts of Quebec and Ontario, in order to analyze their trends. The results of the trend analysis showed that there are positive and negative trends; however, they were dominated mostly by positive trends. In order to determine the most appropriate Daubechies (db) wavelet type and border condition in the DWT procedure, not only were the *MREs* considered, but also the MK *Z*-value relative errors. This additional criterion proposed in this study was found to be very useful because the differences in the $e_r$ were much more noticeable compared to the differences in the *MREs*. In this study, the proposed relative error criterion served as a better indicator in determining the number of decomposition levels, the mother wavelet, as well as the extension border to be used in the data analysis – these is-

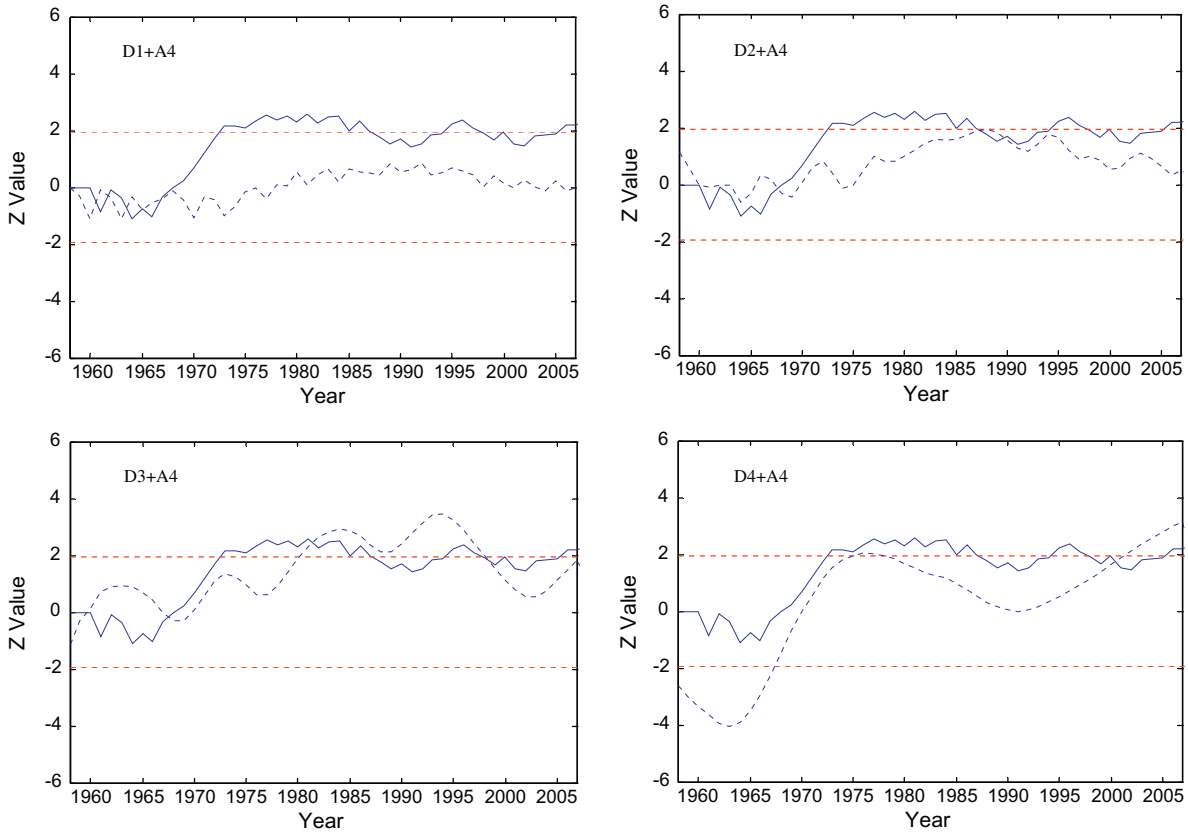


**Fig. 14.** Examples of sequential Mann–Kendall graphs of the detail components of the annual precipitation data in order to determine the most dominant periodicity for trends (Ottawa CDA's data were used in this example). The upper and lower dashed lines represent the confidence limits ($\alpha = 5\%$); the solid and dashed progressive lines are the original and detail sequential MK lines, respectively.

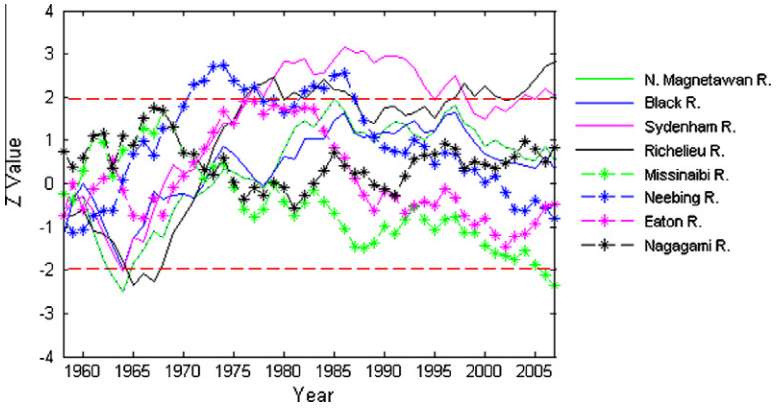


**Fig. 15.** Progressive Mann–Kendall graphs of all the original annual flow data used in the study. The upper and lower dashed lines represent the confidence limits ($\alpha = 5\%$). These graphs were used to determine the possible starting time of the observed trends for the different stations.

sues have not been addressed properly or in any detail in the existing literature.

Although the periodic components that affect the trends are not all the same for all stations, a generalization can be made. For the monthly, seasonally-based, and annual flow data analysis, the most common periodic components that were found to be the most effective in producing the observed trends are 8–32 months, 12–48 months (1–4 years), and 2–4 years, respectively. For the monthly, seasonally-based, and annual precipitation analysis, the periodicities most commonly seen as the most important components are 32-months, 24–48 months (2–4 years), and 2–4 years, respectively. This may be correlated to the NAO cycle because one of the main peaks of the NAO cycles is centered around 2.1 years (Cook et al., 1998; Anctil and Coulibaly, 2004), which seem to coincide with many of the main periodic components of the lower resolution data found in this study. As can be seen, the different data types produced relatively similar conclusions in terms of the most influential periodicities for trends. It may be concluded that for the mean flow and total precipitation over the study area, the trends are influenced by fluctuations of up to 4 years. Although there is a total of 13 stations used in this study, similar conclusions were obtained – this could be attributed by the

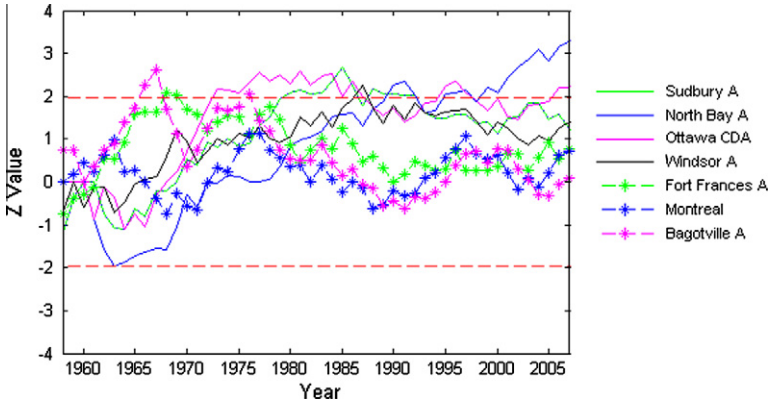


**Fig. 16.** Progressive Mann–Kendall graphs of all the original precipitation data used in the study. The upper and lower dashed lines represent the confidence limits ($\alpha = 5\%$). These graphs were used to determine the possible starting time of the observed trends for the different stations.

fact that the stations are located in relatively close proximity to each other. Therefore, similar climatic factors are affecting the regions in which these stations are located.

The use of the DWT in this study clearly demonstrated how time-scale information can be extracted from a dataset – this information can then be applied to studying how the trends observed in the data were affected by certain time scales. Even for stations that did not exhibit significant trend values for their original data, the decomposition of these data via the DWT was able to identify the time scales that are considered important in affecting the trends. This was accomplished by applying the MK trend tests on the different time modes (detail components). With the sequential MK tests, we were also able to identify the possible starting time in which the trend in a dataset started to appear. In the datasets used in this study, an importance is placed at the time between 1965 and 1970 because most of the trends appeared to start around that time. Anctil and Coulibaly (2004) and Coulibaly and Burn (2004) showed the positive correlation between streamflow/precipitation activities with the PNA cycles since 1970. In this study, most of the flow and precipitation trends started between 1965 and 1970. Fu et al. (2012) also indicated the existence of positive correlations between streamflow in southern Canada and solar activities and El Niño cycles. As can be seen, a number of long-term changes in climate are also factors that may affect the streamflow and precipitation trends over the study area – there is no single factor that acts as the driver for the observed trends over the study area. This is reflected by the different large tele-connection patterns whose cycles seem to coincide with the dominant periodicities. Future studies could incorporate some quantitative linkages between the most dominant periodicities that affect trends (both in flow and precipitation) and the climatic descriptor cycles (or how the combined effects of these climatic descriptors influence the streamflow and precipitation over the study area). This may potentially explain the time–frequency characteristics that affect the trends in streamflow and precipitation over Quebec and Ontario. It would also be beneficial to include more stations from different hydrographic regions within Ontario and Quebec, as well as in other Canadian provinces in order to compare the periodic components that affect the trends in these other areas. Additionally, the implications of these time–frequency characteristics of trends on regional water resources can be looked at in more detail.

Finally, the results obtained from this present study presented some baseline information about the important periodicities that affect the flow and precipitation trends over southern Ontario and Quebec. This information can be integrated into the methods/models aiming to investigate how natural fluctuations (e.g. changes in climate, fluctuations of climate indices, etc.) can affect flow and precipitation trends over southern Ontario and Quebec. Furthermore, the analysis obtained from this study can serve as grounds for basing the water resources design and planning within the watershed covered by the study area, as it involves making reasonable predictions or assumptions about future hydro-climatic conditions.

## Acknowledgements

The authors of this paper would like to thank Dr. Eva Mekis from the Climate Research Division, Environment Canada for providing the second generation adjusted precipitation datasets used in this study. Funding provided by an NSERC Discovery Grant held by Jan Adamowski is also acknowledged.

## References

Abdul Aziz, O.I., Burn, D.H., 2006. Trends and variability in the hydrological regime of the Mackenzie River Basin. J. Hydrol. 319 (1–4), 282–294.
Adamowski, K., Bocci, C., 2001. Geostatistical regional trend detection in river flow data. Hydrol. Process. 15 (18), 3331–3341.
Adamowski, K., Bougadis, J., 2003. Detection of trends in annual extreme rainfall. Hydrol. Process. 17 (18), 3547–3560.
Adamowski, K., Prokoph, A., Adamowski, J., 2009. Development of a new method of wavelet aided trend detection and estimation. Hydrol. Process. 23 (18), 2686–2696.
Ampitiyawatta, A.D., Guo, S., 2009. Precipitation trends in the Kalu Ganga basin in Sri Lanka. J. Agric. Sci. 4 (1), 10–18.
Anctil, F., Coulibaly, P., 2004. Wavelet analysis of the interannual variability in southern Québec streamflow. J. Clim. 17 (1), 163–173.
Assani, A.A., Charron, S., Matteau, M., Mesfioui, M., Quessy, J.-F., 2010. Temporal variability modes of floods for catchments in the St. Lawrence watershed (Quebec, Canada). J. Hydrol. 385 (1–4), 292–299.
Birsan, M.-V., Molnar, P., Burlando, P., Pfaundler, M., 2005. Streamflow trends in Switzerland. J. Hydrol. 314 (1–4), 312–329.
Boyer, C., Chaumont, D., Chartier, I., Roy, A.G., 2010. Impact of climate change on the hydrology of St. Lawrence tributaries. J. Hydrol. 384 (1–2), 65–83.
Bruce, L.M., Koger, C.H., Jiang, L., 2002. Dimensionality reduction of hyperspectral data using discrete wavelet transform feature extraction. IEEE Trans. Geosci. Remote Sens. 40 (10), 2331–2338.
Burn, D.H., Hag Elnur, M.A., 2002. Detection of hydrologic trends and variability. J. Hydrol. 255 (1–4), 107–122.
Burn, D.H., Sharif, M., Zhang, K., 2010. Detection of trends in hydrological extremes for Canadian watersheds. Hydrol. Process. 24 (13), 1781–1790.
Cannas, B., Fanni, A., See, L., Sias, G., 2006. Data preprocessing for river flow forecasting using neural networks: wavelet transforms and data partitioning. Phys. Chem. Earth 31 (18), 1164–1171.
Choi, T.-M., Yu, Y., Au, K.-F., 2011. A hybrid SARIMA wavelet transform method for sales forecasting. Decis. Support Syst. 51 (1), 130–140.
Chou, C.-M., 2007. Applying multi-resolution analysis to differential hydrological grey models with dual series. J. Hydrol. 332 (1–2), 174–186.
Chou, C.-M., 2011. Wavelet-based multi-scale entropy analysis of complex rainfall time series. Entropy 13 (1), 241–253.
Clark, J.S., Yiridoe, E.K., Burns, N.D., Astatkie, T., 2000. Regional climate change: trend analysis of temperature and precipitation series at selected Canadian sites. Can. J. Agric. Econ. 48 (1), 27–38.

Coats, R., 2010. Climate change in the Tahoe basin: regional trends, impacts and drivers. Climatic Change 102 (3), 435–466.
Cook, E.R., D'Arrigo, R.D., Briffa, K.F., 1998. A reconstruction of the North Atlantic Oscillation using tree-ring chronologies from North America and Europe. Holocene 8, 1–9.
Coulibaly, P., Burn, D.H., 2004. Wavelet analysis of variability in annual Canadian streamflows. Water Resour. Res. 40 (3), W03105.
Cunderlik, J.M., Burn, D.H., 2004. Linkages between regional trends in monthly maximum flows and selected climatic variables. J. Hydrol. Eng. 9 (4), 246–256.
Daubechies, I., 1990. The wavelet transform, time-frequency localization and signal analysis. IEEE Trans. Inf. Theory 36 (5), 961–1005.
Daubechies, I., 1992. Ten Lectures on Wavelets. SIAM, Philadelphia.
de Artigas, M.Z., Elias, A.G., de Campra, P.F., 2006. Discrete wavelet analysis to assess long-term trends in geomagnetic activity. Phys. Chem. Earth 31 (1–3), 77–80.
Dietz, E.J., Killeen, T.J., 1981. A nonparametric multivariate test for monotone trend with pharmaceutical applications. J. Am. Stat. Assoc. 76 (373), 169–174.
Dong, X., Nyren, P., Patton, B., Nyren, A., Richardson, J., Maresca, T., 2008. Wavelets for agriculture and biology: a tutorial with applications and outlook. Bioscience 58 (5), 445–453.
Drago, A.F., Boxall, S.R., 2002. Use of the wavelet transform on hydro-meteorological data. Phys. Chem. Earth 27 (32–34), 1387–1399.
Durdu, Ö.F., 2010. Effects of climate change on water resources of the Büyük Menderes River basin, western Turkey. Turk. J. Agric. Forest. 34 (4), 319–332.
Ehsanzadeh, E., Adamowski, K., 2007. Detection of trends in low flows across Canada. Can. Water Resour. J. 32 (4), 251–264.
Ehsanzadeh, E., Ouarda, T.B.M.J., Saley, H.M., 2011. A simultaneous analysis of gradual and abrupt changes in Canadian low streamflows. Hydrol. Process. 25 (5), 727–739.
Fu, C., James, A.L., Wachowiak, M.P., 2012. Analyzing the combined influence of solar activity and El Niño on streamflow across southern Canada. Water Resour. Res. 48 (5), W05507.
Fugal, D.L., 2009. Conceptual Wavelets in Digital Signal Processing: An In-depth, Practical Approach for the Non-mathematician, first ed. Space & Signals Technologies LLC.
Goodwin, D.A., 2008. Wavelet Analysis of Temporal Data. Dissertation, Department of Statistics, The University of Leeds, Leeds, UK.
Groleau, A., Mailhot, A., Talbot, G., 2007. Trend analysis of winter rainfall over southern Québec and New Brunswick (Canada). Atmos. Ocean 45 (3), 153–162.
Hamed, K.H., 2008. Trend detection in hydrologic data: the Mann–Kendall trend test under the scaling hypothesis. J. Hydrol. 349 (3–4), 350–363.
Hamed, K.H., Rao, A.R., 1998. A modified Mann–Kendall trend test for autocorrelated data. J. Hydrol. 204 (1–4), 182–196.
Hirsch, R.M., Slack, J.R., 1984. A nonparametric trend test for seasonal data with serial dependence. Water Resour. Res. 20 (6), 727–732.
Hirsch, R.M., Slack, J.R., Smith, R.A., 1982. Techniques of trend analysis for monthly water quality data. Water Resour. Res. 18 (1), 107–121.
IPCC, 2007. Climate change 2007: the fourth IPCC scientific assessment. In: Parry, M.L., Canziani, O.F., Palutikof, J.P., van der Linden, P.J., Hanson, C.E. (Eds.), Intergovernmental Panel on Climate Change. Cambridge University Press, Cambridge, United Kingdom and New York, NY, USA.
Kallache, M., Rust, H.W., Kropp, J., 2005. Trend assessment: applications for hydrology and climate research. Nonlinear Process. Geophys. 12 (2), 201–210.
Kendall, M.G., 1975. Rank Correlation Methods. Griffin, London, UK.
Kim, S., 2004. Wavelet analysis of precipitation variability in northern California, USA. KSCE J. Civ. Eng. 8 (4), 471–477.
Kisi, O., Cimen, M., 2011. A wavelet-support vector machine conjunction model for monthly streamflow forecasting. J. Hydrol. 399 (1–2), 132–140.
Kulkarni, J.R., 2000. Wavelet analysis of the association between the Southern Oscillation and the Indian summer monsoon. Int. J. Climatol. 20 (1), 89–104.
Kumar, S., Merwade, V., Kam, J., Thurner, K., 2009. Streamflow trends in Indiana: effects of long term persistence, precipitation and subsurface drains. J. Hydrol. 374 (1–2), 171–183.
Labat, D., 2005. Recent advances in wavelet analyses: Part 1. A review of concepts. J. Hydrol. 314 (1–4), 275–288.
Labat, D., Goddéris, Y., Probst, J.L., Guyot, J.L., 2004. Evidence for global runoff increase related to climate warming. Adv. Water Resour. 27 (6), 631–642.
Liu, D., Chen, X., Lian, Y., Lou, Z., 2010. Impacts of climate change and human activities on surface runoff in the Dongjiang River basin of China. Hydrol. Process. 24 (11), 1487–1495.
Mallat, S.G., 1989. A theory for multiresolution signal decomposition: the wavelet representation. IEEE Trans. Pattern Anal. Mach. Intell. 11 (7), 674–693.
Mann, H.B., 1945. Nonparametric tests against trend. Econometrica 13 (3), 245–259.
McBean, E., Motiee, H., 2006. Assessment of impacts of climate change on water resources – a case study of the Great Lakes of North America. Hydrol. Earth Syst. Sci. Discuss. 3 (5), 3183–3209.
Mekis, E., Hogg, W.D., 1999. Rehabilitation and analysis of Canadian daily precipitation time series. Atmos. Ocean 37 (1), 53–85.
Mekis, É., Vincent, L.A., 2011. An overview of the second generation adjusted daily precipitation dataset for trend analysis in Canada. Atmos. Ocean 49 (2), 163–177.
Mishra, A.K., Singh, V.P., 2010. Changes in extreme precipitation in Texas. J. Geophys. Res. 115 (D14), D14106.
Mohsin, T., Gough, W., 2010. Trend analysis of long-term temperature time series in the Greater Toronto Area (GTA). Theor. Appl. Climatol. 101 (3), 311–327.
Nolin, A.W., Hall-McKim, E.A., 2006. Frequency modes of monsoon precipitation in Arizona and New Mexico. Mon. Weather Rev. 134 (12), 3774–3781.
Önöz, B., Bayazit, M., 2003. The power of statistical tests for trend detection. Turk. J. Eng. Environ. Sci. 27 (4), 247.
Partal, T., 2010. Wavelet transform-based analysis of periodicities and trends of Sakarya basin (Turkey) streamflow data. River Res. Appl. 26 (6), 695–711.
Partal, T., Küçük, M., 2006. Long-term trend analysis using discrete wavelet components of annual precipitations measurements in Marmara region (Turkey). Phys. Chem. Earth 31 (18), 1189–1200.
Percival, D.B., 2008. Analysis of geophysical time series using discrete wavelet transforms: an overview. In: Donner, R.V., Barbosa, S.M. (Eds.), Nonlinear Time Series Analysis in the Geosciences – Applications in Climatology, Geodynamics, and Solar-terrestrial Physics. Springer, Berlin/Heidelberg.
Popivanov, I., Miller, R.J., 2002. Similarity search over time-series data using wavelets. In: Proceedings 18th International Conference on Data Engineering, pp. 212–221.
Popoola, A.O., 2007. Fuzzy-wavelet Method for Time Series Analysis. Dissertation, Department of Computing, School of Electronics and Physical Sciences, University of Surrey, Guildford, UK.
Prokoph, A., Adamowski, J., Adamowski, K., 2012. Influence of the 11 year solar cycle on annual streamflow maxima in Southern Canada. J. Hydrol. 442–443, 55–62.
Quiroz, R., Yarlequé, C., Posadas, A., Mares, V., Immerzeel, W.W., 2011. Improving daily rainfall estimation from NDVI using a wavelet transform. Environ. Modell. Softw. 26 (2), 201–209.
Roy, L., Leconte, R., Brissette, F.P., Marche, C., 2001. The impact of climate change on seasonal floods of a southern Quebec river basin. Hydrol. Process. 15 (16), 3167–3179.
Santos, C.A.G., Galvão, C.d.O., Suzuki, K., Trigo, R.M., 2001. Matsuyama city rainfall data analysis using wavelet transform. Annu. J. Hydraul. Eng., JSCE 45, 6.
Shao, Q., Li, Z., Xu, Z., 2010. Trend detection in hydrological time series by segment regression with application to Shiyang River basin. Stoch. Env. Res. Risk Assess. 24 (2), 221–233.
Stone, D.A., Weaver, A.J., Zwiers, F.W., 2000. Trends in Canadian precipitation intensity. Atmos. Ocean 38 (2), 321–347.
Su, H., Liu, Q., Li, J., 2011. Alleviating border effects in wavelet transforms for nonlinear time-varying signal analysis. Adv. Electr. Comput. Eng. 11 (3), 6.
Svensson, C., Kundzewicz, W.Z., Maurer, T., 2005. Trend detection in river flow series: 2. Flood and low-flow index series. Hydrol. Sci. J. 50 (5), 824.
Timofeev, A., Sterin, A., 2010. Using the quantile regression method to analyze changes in climate characteristics. Russ. Meteorol. Hydrol. 35 (5), 310–319.
Torrence, C., Compo, G.P., 1998. A practical guide to wavelet analysis. Bull. Am. Meteorol. Soc. 79 (1), 61–78.
Vonesch, C., Blu, T., Unser, M., 2007. Generalized Daubechies wavelet families. IEEE Trans. Signal Process. 55 (9), 4415–4429.
Wang, W., Hu, S., Li, Y., 2011. Wavelet transform method for synthetic generation of daily streamflow. Water Resour. Manage. 25 (1), 41–57.
Xu, J., Chen, Y., Li, W., Ji, M., Dong, S., Hong, Y., 2009. Wavelet analysis and nonparametric test for climate change in Tarim River basin of Xinjiang during 1959–2006. Chin. Geogr. Sci. 19 (4), 306–313.
Yue, S., Pilon, P., 2004. A comparison of the power of the *t*-test, Mann–Kendall and bootstrap tests for trend detection. Hydrol. Sci. J. 49 (1), 21–37.
Yue, S., Pilon, P., 2005. Probability distribution type of Canadian annual minimum streamflow. Hydrol. Sci. J. 50 (3), 438.
Yue, S., Pilon, P., Phinney, B., Cavadias, G., 2002. The influence of autocorrelation on the ability to detect trend in hydrological series. Hydrol. Process. 16 (9), 1807–1829.
Zhang, X., Vincent, L.A., Hogg, W.D., Niitsoo, A., 2000. Temperature and precipitation trends in Canada during the 20th century. Atmos. Ocean 38 (3), 395–429.
Zhang, X., Harvey, K.D., Hogg, W.D., Yuzyk, T.R., 2001. Trends in Canadian streamflow. Water Resour. Res. 37 (4), 987–998.
Zhang, Q., Xu, C.Y., Zhang, Z., Chen, Y.D., Liu, C.L., 2009. Spatial and temporal variability of precipitation over China, 1951–2005. Theor. Appl. Climatol. 95 (1–2), 53–68.
Zhang, Z., Dehoff, A., Pody, R., Balay, J., 2010. Detection of streamflow change in the Susquehanna River basin. Water Resour. Manage. 24 (10), 1947–1964.
Zume, J., Tarhule, A., 2006. Precipitation and streamflow variability in Northwestern Oklahoma, 1894–2003. Phys. Geogr. 27 (3), 189–205.